Ecotoxicology and Environmental Safety 272 (2024) 116110

Contents lists available at ScienceDirect

Ecotoxicology and Environmental Safety

journal homepage: www.elsevier.com/locate/ecoenv

# Myocardial fibrosis induced by nonylphenol and its regulatory effect on the TGF-β1/LIMK1 signaling pathway

Mei Guo [a,1], Jie Xu [a,1], Xianping Long [b], Weichu Liu [a], Ahmad Zaharin Aris [c], Danli Yang [d], Ya Luo [a], Yuzhu Xu [a], Jie Yu [a,*]

[a] School of Public Health, Zunyi Medical University, Zunyi, Guizhou, 563000, China
[b] Department of Cardiology, Affiliated Hospital of Zunyi Medical University, Guizhou, China
[c] Department of Environment, Faculty of Forestry and Environment, Universiti Putra Malaysia, Serdang, Selangor 43400 UPM, Malaysia
[d] Key Laboratory of Basic Pharmacology of Ministry of Education and Joint International Research Laboratory of Ethnomedicine of Ministry of Education, School of Pharmacy, Zunyi Medical University, Zunyi, Guizhou 563000, China

ARTICLE INFO

Edited by Bing Yan

*Keywords:*
Nonylphenol
Cardiac fibroblasts
Myocardial fibrosis
TGF-β1/LIMK1 signaling pathway

ABSTRACT

*Objective:* We here explored whether perinatal nonylphenol (NP) exposure causes myocardial fibrosis (MF) during adulthood in offspring rats and determined the role of the TGF-β1/LIMK1 signaling pathway in NP-induced fibrosis in cardiac fibroblasts (CFs).
*Methods and results:* Histopathology revealed increased collagen deposition and altered fiber arrangement in the NP and isoproterenol hydrochloride (ISO) groups compared with the blank group. Systolic and diastolic functions were impaired. Western blotting and qRT-PCR demonstrated that the expression of central myofibrosis-related proteins (collagens I and III, MMP2, MMP9, TGF-β1, α-SMA, IL-1β, and TGF-β1) and genes (Collagen I, Collagen III, TGF-β1, and α-SMA mRNA) was upregulated in the NP and ISO groups compared with the blank group. The mRNA-seq analysis indicated differential expression of TGF-β1 signaling pathway-associated genes and proteins. Fibrosis-related protein and gene expression increased in the CFs stimulated with the recombinant human TGF-β1 and NP, which was consistent with the results of animal experiments. According to the immunofluorescence analysis and western blotting, NP exposure activated the TGF-β1/LIMK1 signaling pathway whose action mechanism in NP-induced CFs was further validated using the LIMK1 inhibitor (BMS-5). The inhibitor modulated the TGF-β1/LIMK1 signaling pathway and suppressed the NP-induced increase in fibrosis-related protein expression in the CFs. Thus, the aforementioned pathway is involved in NP-induced fibrosis.
*Conclusion:* We here provide the first evidence that perinatal NP exposure causes myocardial fibrosis in growing male rat pups and reveal the molecular mechanism and functional role of the TGF-β1/LIMK1 signaling pathway in this process.

## 1. Introduction

Fibrosis is a characteristic of most cardiovascular diseases (CVDs) and an end-stage pathological manifestation of various cardiac diseases (Broughton et al., 2018; Park et al., 2018; Travers et al., 2016), such as heart failure (Wang et al., 2020), myocardial infarction (Xiao et al., 2019), and hypertension (Wan et al., 2021). Endocrine-disrupting chemicals (EDCs) are a structurally diverse class of natural or synthetic compounds that can alter various endocrine mechanisms, thereby exerting adverse health effects on exposed individuals and populations. Nonylphenol (NP) is a typical EDC widely used in household and industrial products. NPs are crucial metabolic derivatives of alkylphenols (APs) and alkylphenol ethoxylates (APEs), comprising a complex mixture of branched isomers. These NP isomers demonstrate a spectrum of toxic effects that vary among them (Lu and Gan, 2014). Hence, it is imperative to analyze environmental and human biological samples with isomeric precision to fully understand the distribution, exposure levels, and toxicity of NPs in both ecosystems and human populations. In this study, the focus was on 4-nonylphenol, a NP isomer known for its environmental persistence, showcasing a particularly high affinity for

* Corresponding author.
*E-mail address:* Yujie@zmu.edu.cn (J. Yu).
[1] These two authors contributed equally to this paper.

https://doi.org/10.1016/j.ecoenv.2024.116110
Received 30 May 2023; Received in revised form 23 January 2024; Accepted 11 February 2024
Available online 15 February 2024

adsorption onto soils and sediments. This compound is characterized by its low mobility and biodegradability, combined with high lipophilicity and hydrophobicity, all of which contribute to its longevity in the environment and its elevated toxicity, especially towards aquatic life (Shan et al., 2011). Due to these properties, 4-nonylphenol also represents a substantial risk to human health. According to *in vivo* and *in vitro* studies, EDC exposure can lead to myocardial fibrosis. Short-term bisphenol A (BPA) exposure increased collagen deposition and the expression of pro-fibrotic factor-encoding genes in mouse heart tissue (García-Arévalo et al., 2021a). Additionally, Zhou et al (Zhou et al., 2022). observed that exposure to low cadmium doses during pregnancy caused cardiac dysfunction and increased fibrosis in the offspring. Among other organs, the heart is a vital target organ of NP, and lower NP concentrations increase cardiac contractility and induce direct cardiac toxicity (Gao et al., 2015). However, the toxic mechanism underlying NP's action is unknown. Few large-scale epidemiological studies have investigated the effects of NP on population health. Our population survey revealed that NP, which was commonly detected in the serum of children aged 5–14 years in Zunyi City, Northern Guizhou Province, China, is an environmental risk factor during pregnancy, infancy, and school-age (Fu et al., 2022). In addition, our meta-analysis unveiled that exposure to EDCs, including NP, is a risk factor for CVD. Long-term EDC exposure can influence cardiovascular health in humans (Fu et al., 2020). The heart weight in the offspring is altered by perinatal NP exposure, with specific amounts of NP accumulating in the serum. This suggests that NP is transmitted to infants through the blood–brain barrier (BBB) (Wang et al., 2019; Yu et al., 2017), placenta, or breast milk (Huang et al., 2014), thus causing irreversible damage to their organs (Eisner et al., 2020). We here investigated whether NP exposure causes myocardial fibrosis and determined the underlying pathological mechanisms.

One crucial pathological mechanism underlying myocardial fibrosis development is excessive deposition of the extracellular matrix (ECM). Collagen, matrix metalloproteinases (MMPs), transforming growth factors, and inflammatory factors are key players in maintaining intracellular ECM homeostasis. Because of changes in the levels of these factors, large amounts of ECM are secreted, thereby inducing myocardial fibrosis (Díez et al., 2020; Radhiga et al., 2019). Transforming growth factor-β1 (TGF-β1) critically regulates multiple factors associated with myocardial fibrosis, which causes an imbalance in the collagen/MMP ratio, thus increasing the overexpression of inflammatory factors and inducing the expression of α-SMA, a myofibroblast (MFb) marker. Our group previously reported that exposure to 0.4 mg/kg NP induced excessive collagen I and III deposition in cardiac tissues (Li, 2019). Other studies have reported an increase in TGF-β1 and α-SMA protein and gene expression during myocardial fibrosis in BPA-exposed rats (García-Arévalo et al., 2021b; Patel et al., 2015). In adult mice, the extent of fibrosis in the heart tissue after BPA poisoning positively correlated with MMP2 and MMP9 expression (Kasneci et al., 2017a). In addition, *in vivo* studies have exhibited increased serum expression of the inflammatory factor interleukin-1β (IL-1β) in heavy metal chromium-exposed Chinese field dogs (Lu, 2019). In summary, EDC exposure causes fibrosis in cardiac tissues, which occurs along with the deposition of collagens I and III, MMP2 and MMP9, TGF-β1, IL-1β, and α-SMA.

LIM kinase 1 (LIMK1) is a main effector molecule downstream of TGF-β1, which plays a key role. LIMK1 has proline/serine-rich sequences and regulates the polymerization of the downstream agonist protein filaments through phosphorylation. It has a crucial role in various human diseases. LIMK1 is highly expressed in gastric cancer (Kang et al., 2021), lung cancer (Zhou et al., 2022), and prostate cancer (Huang et al., 2020), and is closely associated with tumor invasion and metastasis. LIMK1 phosphorylates Cofilin, the only known LIMK substrate, to regulate its recombination with actin, thus accelerating cell cycle progression and stimulating cell proliferation (Xie et al., 2017a). LIMK1 was found to be associated with myocardial fibrosis development. For example, Song et al (Song, 2020). observed that the TGF-β1/LIMK1 signaling pathway is involved in myocardial fibrosis, during which LIMK1 and Cofilin (a downstream protein) expression is increased. Moreover, Zhao et al (Zhao et al., 2007). reported that activation of the α-SMA promoter occurs after LIMK1-Cofilin pathway activation, which increases α-SMA expression, leading to fibrosis in cardiac fibroblasts (CFs). Using a combination of biomarkers, the present study for the first time investigated the role of perinatal NP exposure in myocardial fibrosis of adult littermates and that of the TGF-β1/LIMK1 signaling pathway in NP-induced fibrosis in primary CFs. The current study is based on previous studies reporting that NP causes myocardial fibrosis (Liu et al., 2021). We provide a basis for the study of myocardial fibrosis-related diseases caused by NP exposure, potential targets and new ideas for the further treatment of EDC-induced heart-related diseases, and a theoretical framework for future research into new therapeutic drugs for use against myocardial fibrosis in clinics.

## 2. Methods

### 2.1. Reagents and equipments

The nonylphenol (98% > purity, Product Code: 25154–52–3) was purchased from the Shandong Xiya Chemical Industry Co., Ltd. (Shandong, China). BCA protein Quantitation Kit were purchased from the U. S. Thermo Fisher Scientific Co., Ltd. (New York, USA). Anti-Collagen I, Anti-Collagen III, Anti-MMP2, Anti-MMP9, Anti-alpha smooth muscle Actin, Anti-TGF beta 1, Anti-IL-1beta, Goat Anti-Rabbit IgG H&L (HRP), Anti-Vimentin, Anti-S100A4, Anti-ROCK2+ROCK1 and Anti-RhoA were purchased from Abcam (Cambridge, USA). Anti-TGF beta1 Ab, Anti-LIMK1 Ab, Anti-Phospho-LIMK1 ( Thr508 ) Ab, Anti-Cofilin Ab and Anti-Phospho- Cofilin ( Ser3 ) Ab were purchased from Affinity Biosciences (Jiangsu, China). All primer sequences were purchased from Sangon Biotech (Shanghai, China). PrimeScriptTM RT Master Mix and SYBR® Premix Ex TaqTMII were purchased from Takara (Shiga, Japan). Isoproterenol hydrochloride and type II collagenase were purchased from Sigma (New York, USA). Recombinant human TGF-β1 were purchased from PEPROTECH (New Jersey, USA). Fetal calf serum were purchased from Biological industries (Kibbutz Beit Haemek, Israel). HP-1100 High Performance Liquid Chromatography (HPLC) was purchased from the Agilent Technologies (Palo Alto, CA, USA). ChemiDocTM Touch imaging system was purchased from BIO-RAD (California, USA). Fluorescence microscope was purchased from Olympus (Tokyo, Japan). All other chemicals were commercially available. High Resolution Imaging System (VEVO 2100) were purchased from Canada (Toronto, Canada).

### 2.2. Experimental animal feeding and grouping

Sixty Sprague-Dawley (SD) rats (age: 2 months; females: 48; males: 12) were obtained from Hunan SJA Laboratory Animal Co., Ltd [License number: SCXK (Xiang) 2019–0004], acclimatized, and fed for 1 week. At 8:00 pm daily, the rats from different cages were shuffled and placed back in the cages at a 2:1 male to female ratio. Vaginal smears of the rats were obtained before 8:00 am the next day. Spermatozoa in the smears were observed under the microscope. If conception was confirmed, this was considered as the first day of pregnancy. The pregnant rats were randomly assigned to five groups: blank (corn oil), NP (2.5 mg/kgbw/day, 50 mg/kgbw/day, and 100 mg/kgbw/day), and model. These rats were gavaged with 5 mL/kg NP at 9:00 am daily starting from day 1 of gestation until 21 days after delivery (weaning period). The tolerable daily doses of NP for Chinese individuals and rats are 0.025 mg/kgbw and 2.5 mg/kg [TDI × 100 (species and genus coefficient 10 × uncertainty coefficient 10)], respectively (Chen et al., 2018). The maximum no-observed-adverse-effect-level (NOAEL) of NP in parent and offspring rats is 50 mg/kg (Cunny et al., 1997; Nagao et al., 2001). Histopathological results of female adult offspring rats exposed to dimethyl phthalate (100 mg/kg) through the uterus have revealed the presence of

disorderedly arranged myocardial fibers (Zhao, 2014). Meanwhile, exposure to 100 mg/kg/day NP during the perinatal period exacerbates asthma and causes neurotoxicity in the offspring (Yu et al., 2020b, 2016). After the rats were weaned, two male offspring rats were randomly selected from each litter of offspring rats and categorized into dose-based groups, with each group containing 18 rats. All rats were raised in a standardized animal room environment (at a temperature of 25℃ ± 3℃, humidity of 55℃ ± 5℃, and a 12 h light/dark cycle) and given free access to water and feed according to their weights (8 g/100 g). At 24 h after the last drug administration, the rats were anesthetized using 10% ethyl carbamate. Their heart samples were collected, perfused with phosphate buffer, dried using a filter paper, weighed using an electronic balance, and stored at −80℃. All biological replicates were generated using male offspring rats from different litters. Animal experiments were approved by the Ethics Committee of Zunyi Medical University [No. Lun Shen (2020) 2–359].

### 2.3. Myocardial fibrosis model

We used 70 SD rats (age: 5 days) as offspring for model development. Dorsal subcutaneous injections of isoproterenol hydrochloride (ISO) were administered at a volume of 1 mL/100 g to develop a myocardial fibrosis model (Chen et al., 2018). On different days, the ISO doses varied: 25 mg/kg on day 1, 20 mg/kg on day 2, 15 mg/kg on day 3, 10 mg/kg on day 4, 5 mg/kg on day 5, and continued at 5 mg/kg until day 15 (Fig. 1-A). Heart samples were obtained on day 16. The successful establishment of the myocardial fibrosis model was verified by performing Van Gieson (VG), Masson trichrome, and Sirius Red staining after modeling.

### 2.4. Doppler ultrasound monitoring of cardiac function

Ninety-day-old male offspring rats exposed to NP during the perinatal period were anesthetized with 10% urethane (6 animals per group). Subsequently, parameters such as fractional shortening (FS), ejection fraction (EF), left ventricular (LV) forearm end-diastolic thickness (LVAWd), LV forearm end-systolic thickness (LVAWs), LV posterior wall end-diastolic thickness (LVPWd), and LV posterior wall end-systolic thickness (LVPWs) were measured using a high-resolution animal ultrasound imaging system (Liu et al., 2021).

### 2.5. Determination of NP accumulation in the serum and heart tissues of rat pups through high-performance liquid chromatography

Ventricular tissue (50 mg) and serum (0.5 mL) were placed in a glass centrifuge tube. Then, 4 mL of hexane and ether mixture ($V_{Hexane}$:$V_{Ether\ mixture}$ = 7:3) was added to the tube. The heart tissue was homogenized for 15 s, followed by shaking and centrifugation (4000 rpm/min,10-min). The supernatant was evaporated in a constant temperature water bath (50°C). The precipitate/pellet was dissolved in 500 μL acetonitrile, filtered through a 0.22-μm organic filter tip, and analyzed using high-performance liquid chromatography (HPLC) for NP detection. The chromatographic conditions established were as follows: mobile phase (acetonitrile:0.1% glacial acetic acid = 85:15), injection volume (10 μL),

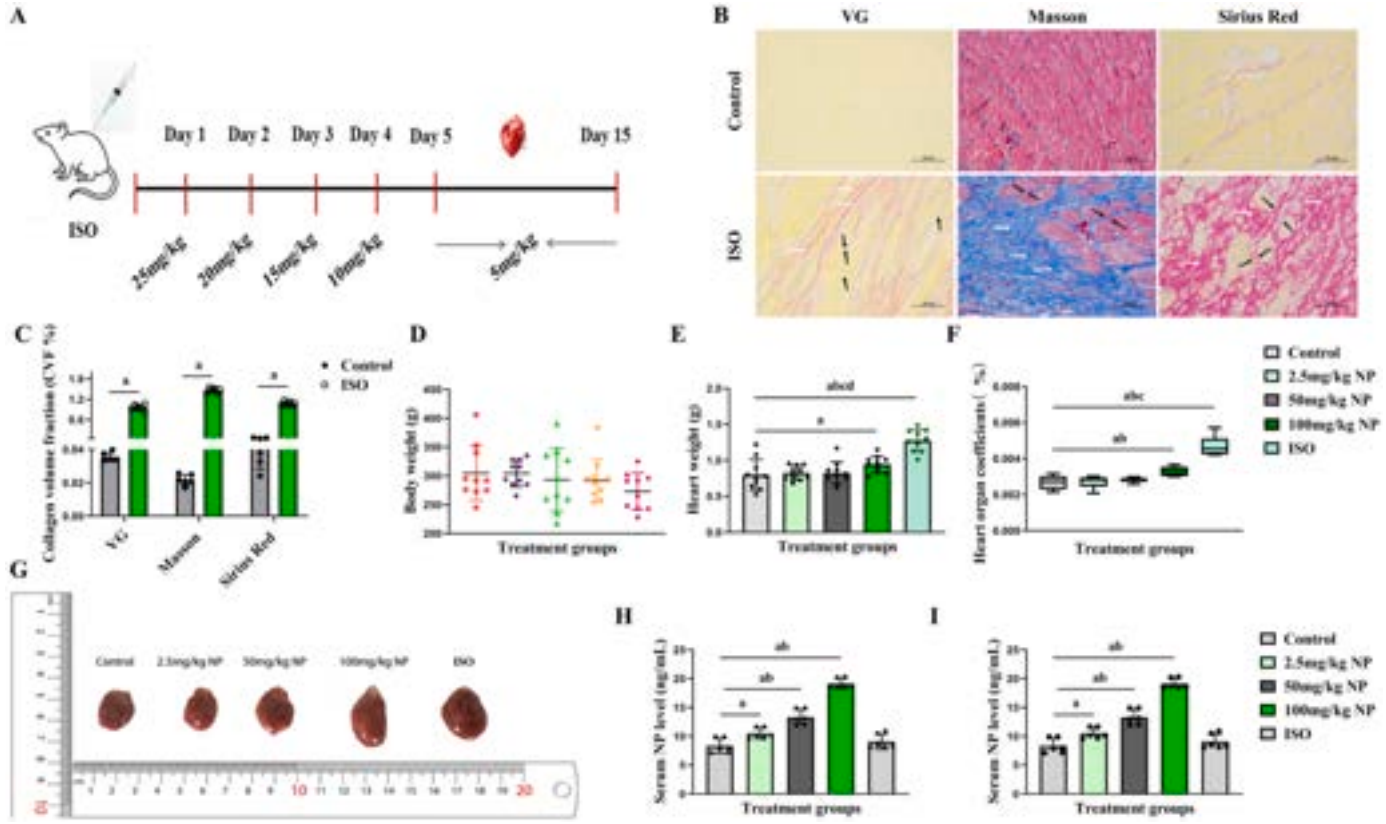


**Fig. 1.** Myocardial fibrosis modeling and detection of fundamental indicators based on 90-day-old rat offspring. A: Rats injected subcutaneously with ISO dorsally for 15 days. B: VG, Masson, and Sirius Red staining (scale bar: 50 μm), red collagen fibers in VG and Sirius Red staining, blue collagen fibers in Masson staining). C: Quantitative analysis of VG, Masson, and Sirius Red staining, n = 6 ($F_{VG}$ = 8.234, $P$ = 0.017; $H_{Masson}$ = 19.844, $P$ = 0.001; $F_{Sirius\ Red}$ = 8.234, $P$ = 0.017). D, E, F: Changes in body weight, heart weight, and organ coefficients, respectively, among the 90-day-old rats in the litter, n = 10 ($F_{heart\ weight}$ = 16.833, $P$ = 0.004; $H_{organ\ coefficients}$ = 35.331; $P$ < 0.001). G: Visualization of heart tissue of 90-day rat pups. H, I: NP accumulation in serum and tissues of adult rats after perinatal NP exposure, n = 6 ($F_{serum}$ = 86.833, $P$ < 0.001; $H_{tissue}$ = 26.524, $P$ < 0.001). Data in C were analyzed via independent samples t-test. Data in E, H and I were analyzed via one-way ANOVA, and comparative analysis was performed via LSD. Data in F was analyzed via Kruskal-Wallis test. Data were expressed as $\overline{X} \pm$ SD. [a]vs Control group, $P$ < 0.05; [b]vs 2.5 mg/kg NP, $P$ < 0.05; [c]vs 50 mg/kg NP, $P$ < 0.05.

column temperature (40°C), wavelength (excitation wavelength: 275 nm; emission wavelength: 312 nm), and flow rate (1 mL/min) (Wang et al., 2021).

### 2.6. Masson trichrome and Sirius Red staining of heart tissues derived from 90-day-old rats to observe collagen deposition

The hearts of the 90-day-old male offspring rats were rapidly isolated on ice. The blood vessels and ears of the rats were clipped. PBS was injected along the vessels into the ventricular chambers for lavage. The tissue was gradually dehydrated with 70%, 80%, 90%, and 95% xylene, and anhydrous ethanol, embedded in paraffin, and cut into 4-μm-thick sections.

For Masson trichrome staining, the sections were treated with Masson composite blue stain solution for 10 min, rinsed rapidly with pure water, soaked in 1% phosphotungstic acid for 5 min, and retained with aniline blue for 3 min. Then, 1% glacial acetic acid was used for 1 min to detect differentiation, followed by treatment with 95% ethanol and anhydrous ethanol for dehydration in sequence and twice with xylene.

During Sirius Red staining, the sections were treated with saturated picric acid Sirius Red stain solution for 10 min, followed by rinsing in anhydrous ethanol for 5 min. The rinsing effects were observed under the microscope. Next, the sections were transferred to an oven at 60°C for 30 min and subjected to transparent treatment in xylene for 5 min.

For VG staining, the specimens were treated with the VG staining solution for 5–10 min, followed by discarding the staining solution and its direct replacement with 95% ethanol for rapid dehydration and xylene for transparency. Finally, the slices were sealed with neutral gum and imaged microscopically. The blue color in Masson trichrome staining and the red color in VG and Sirius Red staining denote collagen fibers. Using Image J software, the collagen volume fraction was calculated by dividing the positive area by the total area (Li et al., 2019).

### 2.7. Immunohistochemical staining of collagen I and III expression in the heart tissue of adult littermates

The tissue slices were dewaxed and subjected to antigen repair. The tissue slices were washed with PBS and incubated with primary antibody (collagen I = 1:200, collagen III = 1:500) overnight, following incubation with BSA blocking solution and washing. The next day, the slices were again washed with PBS, incubated with a secondary antibody, washed, dried, treated with the color development solution, and washed with water. Hematoxylin re-staining and washing were repeated until the blue color returned. Gradient dehydration was performed, and the slices were sealed, analyzed, and imaged microscopically.

### 2.8. Transmission electron microscopy of myocardial fibers and ultrastructure

Hearts of the 90-day-old male offspring rats were perfused with pre-cooled PBS, and a 1-$mm^3$-sized tissue block was obtained from the ventricular portion of the fresh heart tissue. The tissue block was treated with an electron microscope fixative. Following fixation with osmium, ethanol dehydration, acetone treatment, and infiltration with an embedding agent, the sections were stained with uranyl acetate saturated alcohol solution and lead citrate solution, and washed with pure water. The myocardial ultrastructure was observed through transmission electron microscopy (TEM) (Jiang et al., 2021).

### 2.9. Extraction, passaging, and identification of primary CFs

Hearts were stripped from 1- to 3-day-old suckling rats, cut into approximately 1-$mm^3$ tissue pieces and digested with 0.1% type II collagenase at 37°C for 10 min. The supernatant was collected and terminated by adding 10% FBS complete medium at a 1:1 ratio. The digestion process was repeated until the tissue block was completely digested. Following digestion, the mixture was filtered through a 200-mesh cell sieve. The filtrate was centrifuged at 1200 rpm for 5 min, and the resulting supernatant was discarded. The complete medium was added to the cell precipitate and subsequently dispensed in Petri dishes or culture flasks for further incubation (37℃,90 min). After 90 min of cell apposition, the cells were washed 2–3 times with PBS, followed by the addition of a new medium for culture (Li et al., 2020).

CFs were passaged at 80%–90% confluence, and 0.08% trypsin was added for cell digestion. Passaging was performed at a 1:2 ratio. The CFs were identified through immunofluorescence staining with vimentin. The FSP-1 expression rate was ≥95%, and the α-SMA positivity rate was <5% as appropriate.

### 2.10. CCK8 assay of the proliferative effect of recombinant human TGF-β1 on CFs

Ninety-six-well plates were seeded with $1 \times 10^4$/well of CFs, and the cells were allowed to grow overnight. Further, the CFs were treated with 0, 5, and 10 ng/mL of recombinant human TGF- β1 for 12 and 24 h, respectively. Cell proliferation was then detected through the CCK8 assay.

### 2.11. CCK8 assay of growth inhibitory effects and duration of NP exposure in CFs

First, $1 \times 10^4$/well of CFs was seeded into 96-well plates. At approximately 80% cell confluence, the medium was aspirated and the medium containing different NP concentrations (0, 1.25, 2.5, 5, 10, 20, 40, 80, and 100 μM) was added. The plates were incubated for 24 h. Three replicates were established for each concentration. Then, 10 μL CCK8 was added to each well, and the absorbance at 450 nm was measured after 2.5 h. The cell inhibition rate was calculated based on the results. The cells were treated with the optimal NP staining dose for 6, 12, 24, 48, and 72 h. The absorbance values were measured by adding CCK8 to determine the optimal exposure time of NP.

### 2.12. Immunofluorescence detection of myocardial fibrosis-related protein expression

The cells on the crawling slices grew to approximately 70%–80% confluence. The crawling slices were removed for immunofluorescence experiments, following different experimental treatments. The cells were fixed with paraformaldehyde for 20 min, blocked with 5% goat serum for 30 min, and incubated with primary antibodies [collagen I (1:100), collagen III (1:100), MMP2 (1:200), MMP9 (1:100), TGF-β1 (1:100), α-SMA (1:50), P-LIMK1 (1:50), P-Cofilin (1:100), vimentin (1:250), and FSP-1 (1:50)] overnight. The following day, the slices were washed with PBST and incubated with secondary antibodies for 1 h in the dark. Following PBST washing (5 min × 3 times) of the slices, nuclei were stained with DAPI for 10 min. The slices were sealed with an anti-fluorescence attenuator. Finally, the image acquisition was performed under fluorescence microscopy (Medzikovic et al., 2021).

### 2.13. Determination of the expression of myocardial fibrosis-related proteins through western blotting

Total proteins in the cardiac tissues and CFs were extracted using a lysis solution containing RIPA, PMSF, and protease inhibitors at a 100:1:1 ratio for 30 min (Chowdhury and Hell, 2019). The lysate was centrifuged (12,000 rpm, 20 min), and the protein concentration was measured using the BCA protein assay kit. First, up to 40 μg of protein was sampled for electrophoresis. Then, the separated protein bands were electrophoretically transferred to a PVDF membrane. The membrane was treated with 5% BSA to block nonspecific binding. Corresponding bands were cut-off according to the target protein's molecular weight and incubated with primary antibodies overnight at 4℃. The next day,

the antibody incubation kit was removed and left at room temperature for 1 h. The membrane was washed with TBST (5 min × 4 times), incubated with secondary antibodies for 1 h, correspondingly, washed again with TBST (5 min × 4 times), and exposed to the luminescent solution. The protein bands were quantified using Image J software (Yu et al., 2020c).

### 2.14. qRT-PCR for detecting the expression of myocardial fibrosis-related genes

By using the TRIzol method, total RNA was extracted from cardiac tissues and cells. The tissues and cells were lysed with TRIzol and centrifuged (37℃, 10 min, 12,000 rpm). RNA was extracted with chloroform and precipitated with isopropanol. Then, 30–50 μL DEPC water was added to the precipitate. RNA purity was determined based on an $OD_{260}/OD_{280}$ value ranging between 1.9 and 2.1, and an $OD_{260}/OD_{230}$ value of >2. The obtained RNA was reverse-transcribed to cDNA. qRT-PCR was performed using a TB Green kit. GAPDH was the internal control, and the primer sequences are shown in Table 1. The amplification conditions were as follows: pre-denaturation at 95°C for 30 s, 1 cycle; denaturation at 95°C for 5 s, annealing at 60°C for 30 s, and extension at 72°C for 15 s, 40 cycles. Each reaction was repeated three times, and data were obtained using the $2^{-\Delta CT}$ method (Yu et al., 2020a).

### 2.15. RNA-seq transcriptome sequencing for enriching differentially expressed signaling pathways

Three heart tissue samples were obtained from the 90-day-old male offspring rats in the blank group, 100 mg/kg NP group, and ISO group, respectively. RNA was isolated from these samples and purified using the TRIzol method. The amount, purity, and integrity of total RNA were analyzed using NanoDrop ND-1000 and Bioanalyzer 2100. Subsequent experiments were deemed successful if the total RNA was greater than 1 μg; the concentration was greater than 50 ng/μL, and the RIN value was >7.0. The mRNA with polyA tails (polyadenylate) was captured using oligo (dT) magnetic beads, fragmented at 94°C for 5–7 min, and subsequently synthesized into cDNA by using reverse transcription reagents. A strand-specific library with a fragment size of 300 bp ± 50 bp was constructed by following a series of screening and purification steps. Finally, using the sequencing mode PE150, double-end sequencing was performed by Hangzhou Lianchuan Biotechnology Co.

### 2.16. Statistical analysis

Statistical analysis was performed using SPSS 18.0. The data were tested for normality. The chi-square test and independent samples t-test were conducted to analyze the two groups exhibiting normal distribution. One-way ANOVA was performed to analyze multiple groups, and LSD was applied for two-way comparison. The Kruskal–Wallis test was conducted to analyze non-normally distributed data or if the variance was non-homogeneous. All data were expressed as mean ± standard deviation ($\overline{X} \pm SD$). $P < 0.05$ was considered statistically significant. Statistical plots were drawn using GraphPad Prism 8.4 software.

**Table 1**
Primer sequences.

| ID | Gene Name | Sequences ( 5′- 3′ ) | ProdSize |
|---|---|---|---|
| 12842 | Collagen I | Forward TGTTGGTCCTGCTGGCAAGAATG<br>Reverse GTCACCTTGTTCGCCTGTCTCAC | 145 |
| 12825 | Collagen III | Forward AGTCGGAGGAATGGGTGGCTATC<br>Reverse CAGGAGATCCAGGATGTCCAGAGG | 89 |
| 21803 | TGF-β1 | Forward GACCGCAACAACGCAATCTATGAC<br>Reverse CTGGCACTGCTTCCCGAATGTC | 94 |
| 11475 | α-SMA | Forward TGGCCACTGCTGCTTCCTCTTCTT<br>Reverse GGGGCCAGCTTCGTCATACTCCT | 152 |
| 24383 | GAPDH | Forward GACATGCCGCCTGGAGAAAC<br>Reverse AGCCCAGGATGCCCTTTAGT | 92 |

## 3. Results

### 3.1. Myocardial fibrosis modeling and detection of fundamental indicators

Myocardial fibrosis was induced by administering a dorsal subcutaneous injection of ISO to the rats for 15 days (Fig. 1-A). The cardiac tissues were stained with VG, Masson trichrome, and Sirius Red to verify the successful establishment of the myocardial fibrosis rat model. The collagen content in the ISO group was higher than that in the blank group (Fig. 1-B, C). The echocardiogram revealed an increase in the LV wall thickness (Fig. 2-G). TEM images displayed that, compared with the blank group, myogenic fibers in the ISO group were disorganized with unclear Z-lines (white arrows) and their mitochondria had vacuolar-like lesions and were irregularly arranged (red arrows) (Fig. 3-G). Taken together, these results indicated that myocardial fibrosis was successfully induced in the rat models.

Body weight and heart weight are crucial physiological indicators of organism development. Heart tissues of the NP-exposed 90-day-old rat pups in each dose group were smoothly colored, without bleeding spots, while the 100 mg/kg NP and ISO groups exhibited significantly increased heart size and heart-to-body ratio compared with the blank group (Fig. 1-E, F). The body weight of the 90-day-old rats decreased with an increase in dose, but this decrease was not statistically significant between the groups (Fig. 1-D). To explore whether NP was transmitted to the offspring through the BBB, placental barrier, and milk, NP accumulation in the body was measured in the 90-day-old litter through HPLC. The NP content increased as the dose increased and was significantly higher in the 50 and 100 mg/kg NP groups than in the blank and 2.5 mg/kg NP groups (Fig. 1-H, I). Thus, we deduced that NP may be transferred to the offspring via the BBB, placental barrier, and breast milk.

### 3.2. Effects of perinatal NP exposure on the cardiac function of male adult rats

We investigated whether perinatal NP exposure caused cardiac dysfunction in 90-day-old rat pups. The LVFS and LVEF values reduced, which reflected cardiac dysfunction of the littermates (Fig. 2-A, B), whereas those of LVAWs, LVAWd, LVPWs, and LVPWd were higher in the NP groups than in the blank group. Left ventricle thickening was detected with an increase in the NP dose (Fig. 2-C, D, E, F), which indicated that NP exposure resulted in cardiac dysfunction in adult rats.

### 3.3. Pathological tests in 90-day offspring rats

The histopathological results revealed that the content of blue and red collagen fibers increased as the NP dose increased compared with the blank group (Fig. 3-A, B). The 50 and 100 mg/kg NP groups had broken myocardial fibers that were not aligned with the nucleus. The central myocardial fibers in the ISO group were severely disorganized, and the breaks were more obvious (black arrows) (Fig. 3-E, F). The ultrastructure displayed that compared with the blank group, no abnormal fiber arrangement was observed in the 2.5 and 50 mg/kg NP groups, whereas vacuolization was observed in specific mitochondria. Some myogenic fibers in the 100 mg/kg NP group exhibited lysis, disorganized arrangement, and fracture, as well as increased mitochondrial vacuolation; with the degree of fibrosis increasing in severity with an increase in the dose (Fig. 3-G). Additionally, immunohistochemical results revealed that collagen I and III protein expression increased as the NP doses increased (Fig. 3-C, D, H). These results suggested that perinatal NP exposure may cause collagen deposition and fibrous

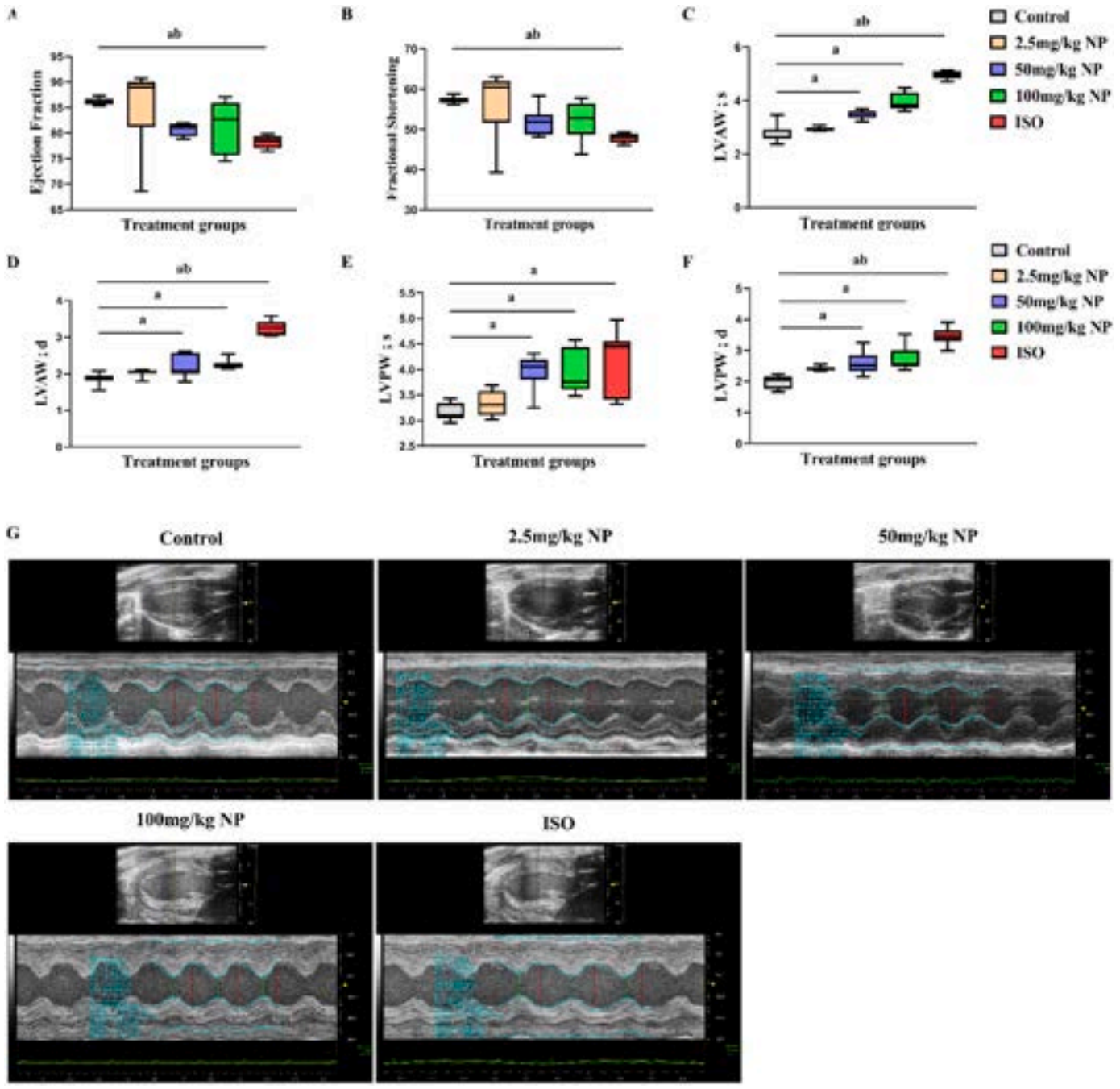


**Fig. 2.** Effects of perinatal NP exposure on the cardiac functions of male adult rats. A: EF changes in each group of male rat pups at 90 days, n = 6 (H = 13.754, $P$ = 0.008). B: Changes in Fs in male pups at 90 days, n = 6 (H = 13.599, $P$ = 0.009). C: Changes in LVAWs in each group of 90-day-old male rat pups, n = 6 (F = 88.955, $P < 0.001$). D: Changes in LVAWd in each group of 90-day-old male rat pups, n = 6 (H = 24.686, $P < 0.001$). E: Changes in LVPWs in each group of 90-day-old male rat pups, n = 6 (H = 24.487, $P < 0.001$). F: Changes in LVPWd in each group of 90-day-old male rat pups, n = 6 (F = 18.175, $P < 0.001$). Echocardiograms of 90-day male rat pups in each group. Data analyzed by Kruskal-Wallis test. Data were expressed as $\overline{X} \pm$ SD. [a]vs Control group, $P < 0.05$; [b]vs 2.5 mg/kg NP, $P < 0.05$; [c]vs 50 mg/kg NP, $P < 0.05$; dvs 100 mg/kg NP, $P < 0.05$.

disorganization in the heart tissue of male adult littermates.

### 3.4. Expression of myocardial fibrosis-related proteins and genes in offspring rats after perinatal NP exposure

The effect of NP exposure on the abnormal expression of myocardial fibrosis-related genes and proteins in 90-day-old male offspring rats was further explored. In our initial study, the protein expression of collagens I and III, MMP2, MMP9, TGF-β1, α-SMA, and IL-1β was higher in the NP and ISO groups than in the blank group, suggesting that NP exposure causes excessive collagen deposition; disruption of MMP2 and MMP9 homeostasis; and overexpression of TGF-β1, IL-1β, and the MFb marker α-SMA (Fig. 4-A–J). To further determine whether NP causes myocardial fibrosis, myocardial fibrosis-related transcription of genes (collagens I and III, TGF-β1, and α-SMA) was assessed. Compared with the blank group and 2.5 and 50 mg/kg NP groups, the 100 mg/kg NP and ISO groups exhibited significantly elevated mRNA expression of collagens I and III, TGF-β1, and α-SMA (Fig. 4-K–N).

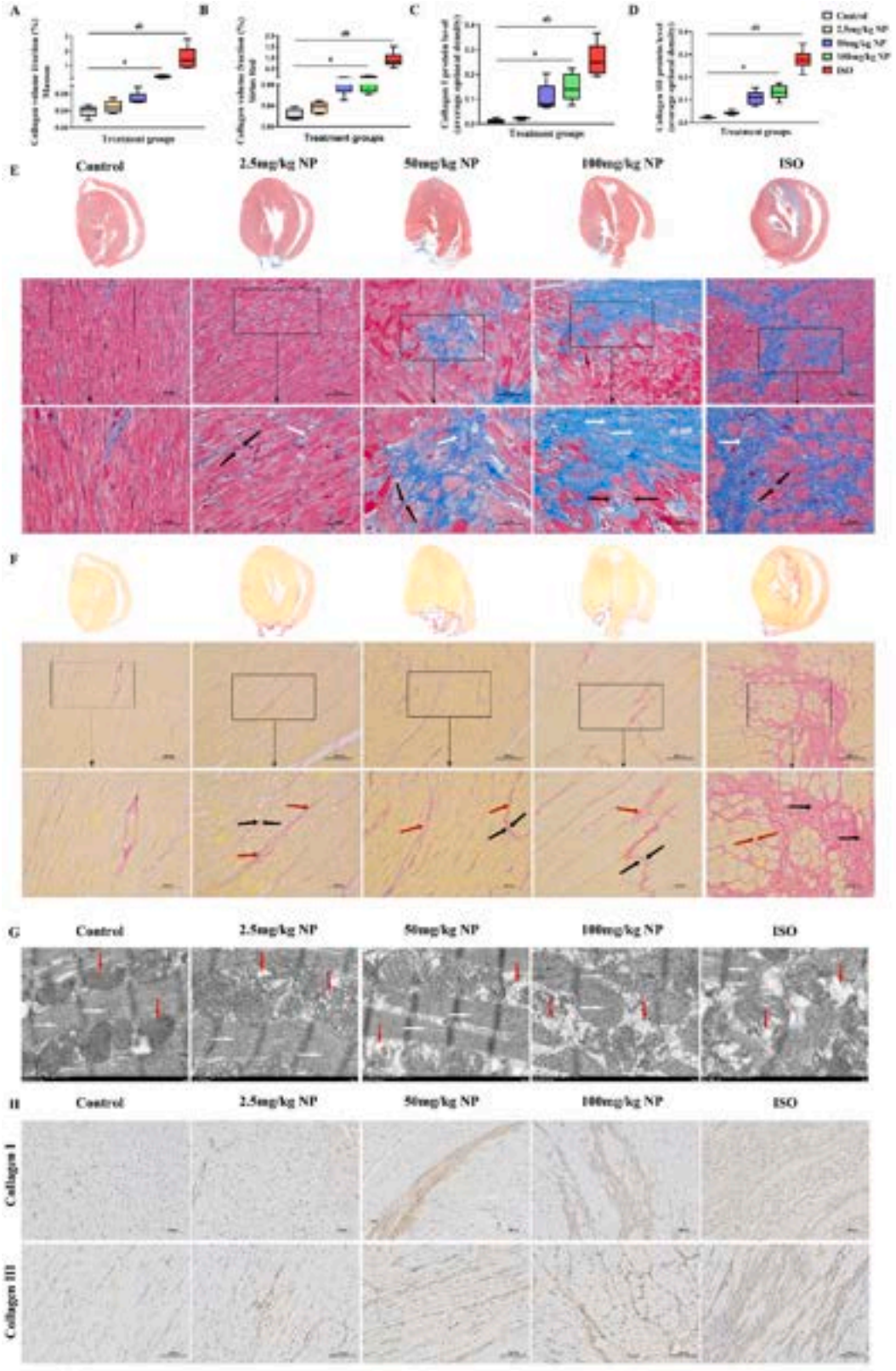


**Fig. 3.** Pathological tests of 90-day offspring rats. A: Masson staining quantitative analysis (CVF (%) = positive area/total area), n = 6 (H = 25.726, $P < 0.001$). B: Quantitative analysis of Sirius Red staining (CVF (%) = positive area/total area), n = 6 (H = 25.880, $P < 0.001$). C: Collagen I protein expression, n = 6 (H = 25.726, $P < 0.001$). D: Collagen III protein expression, n = 6 (H = 25.726, $P < 0.001$). E: Masson staining of heart tissue in 90-day-old male rat pups (left: heart scan; middle: 200 ×; right: 400 ×). F: Sirius Red staining of heart tissues obtained from 90-day-old male rat pups (left: heart scan; middle: 200 ×; right: 400 ×). G: Transmission electron micrographs of myocardial tissue of 90-day-old rats (red arrows: mitochondrial vacuolization; white arrows: Z-line position). H: Immunohistochemistry of collagen I and III (positive expression is indicated by tan color, whereas no color suggested absence of expression). Data in A, B, C and D were analyzed via Kruskal-Wallis test. Data were expressed as $\overline{X} \pm$ SD. [a]vs Control group, $P < 0.05$; [b]vs 2.5 mg/kg NP, $P < 0.05$.

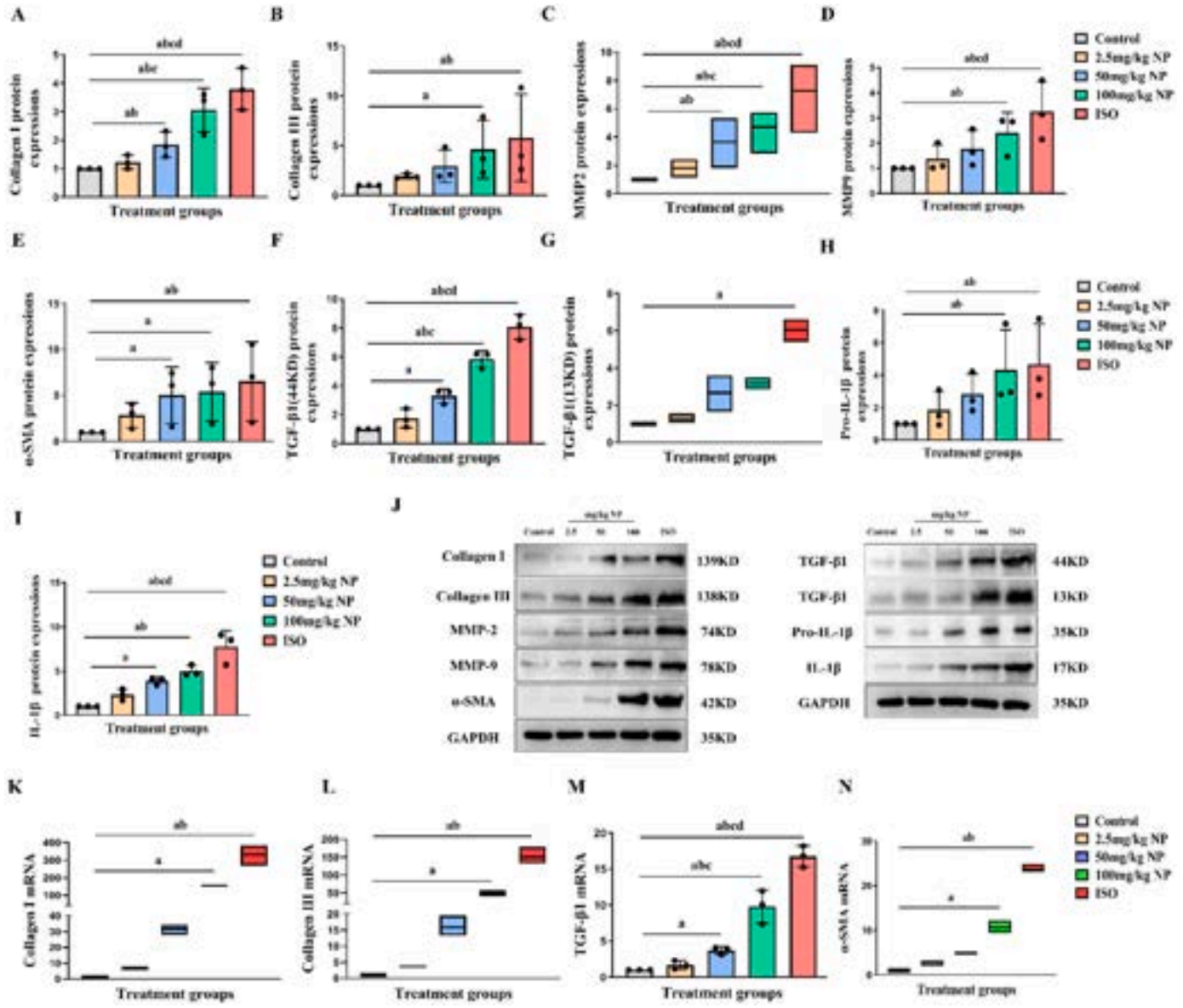


**Fig. 4.** Expression of proteins and genes associated with myocardial fibrosis in offspring rats after perinatal NP exposure. A: Collagen I protein expression, n = 3 (F = 145.385, $P < 0.001$). B: Collagen III protein expression, n = 3 (F = 9.803 , $P = 0.002$). C: MMP2 protein expression, n = 3 (H = 13.233 , $P = 0.01$). D: MMP9 protein expression, n = 3 (F = 24.323, $P < 0.001$). E: α-SMA protein expression, n = 3 (F = 9.659, $P = 0.002$). F: TGF-β1 44KD protein expression, n = 3 (F = 78.628, $P < 0.001$). G: TGF-β1 13KD protein expression, n = 3 (H = 36.389, $P = 0.012$). H: Pro-IL-1β protein expression, n = 3 (F = 9.532, P = 0.002). I: IL-1β protein expression, n = 3 (F = 36.389, P < 0.001). J: Myocardial fibrosis-associated protein expressions in western blot analysis. K: Collagen I mRNA expression, n = 3 (H = 13.597 , $P = 0.009$). L: Collagen III mRNA expression, n = 3 (H = 13.597, $P = 0.009$). M: TGF-β1 mRNA expression, n = 3 (F = 136.895, $P < 0.001$). N: α-SMA mRNA expression, n = 3 (F = 384.614, $P < 0.001$). C, G, K, L and N data were analyzed using Kruskal-Wallis test. A, B, D, E, F, H, I and M data were analyzed via one-way ANOVA, and comparisons between two were analyzed by LSD. Data were expressed as $\overline{X} \pm SD$. [a]vs Control group, $P < 0.05$; [b]vs 2.5 mg/kg NP, $P < 0.05$; [c]vs 50 mg/kg NP, $P < 0.05$.

### *3.5. Kyoto Encyclopedia of Genes and Genomes (KEGG) and Gene Ontology (GO) enrichment analyses of signaling pathways associated with myocardial fibrosis and differential expression*

NP exposure caused myocardial fibrosis in adult offspring rats. To study its underlying mechanism, heart tissue samples in the control group, NP (100 mg/kgbw/day) group, and ISO group were subjected to RNA-sequencing. The results revealed that the fibrosis-related factors and signaling pathways were differentially expressed among the three groups in the Gene Ontology (GO) functional enrichment analysis and Kyoto Encyclopedia of Genes and Genomes (KEGG) signaling pathway enrichment analysis. The GO function was enriched in myocardial fibrosis-associated factors, including inflammatory response, collagen-containing ECM synthesis, TGF-β1 signaling pathway, actin filament binding, and protein serine/threonine kinase activity. Additionally, we focused on myocardial fibrosis-associated signaling pathways. The KEGG results unveiled differential expression of the TGF-β1 signaling pathway, and further enrichment revealed LIMK1 as a related downstream effect factor of TGF-β1. Hence, the TGF-β1/LIMK1 signaling pathway seems to be related to myocardial fibrosis development (Fig. 5-A–E).

### *3.6. Identification of primary CFs*

Primary CFs were used to elucidate the mechanism of NP-induced myocardial fibrosis. After 90 min of differential apposition of the

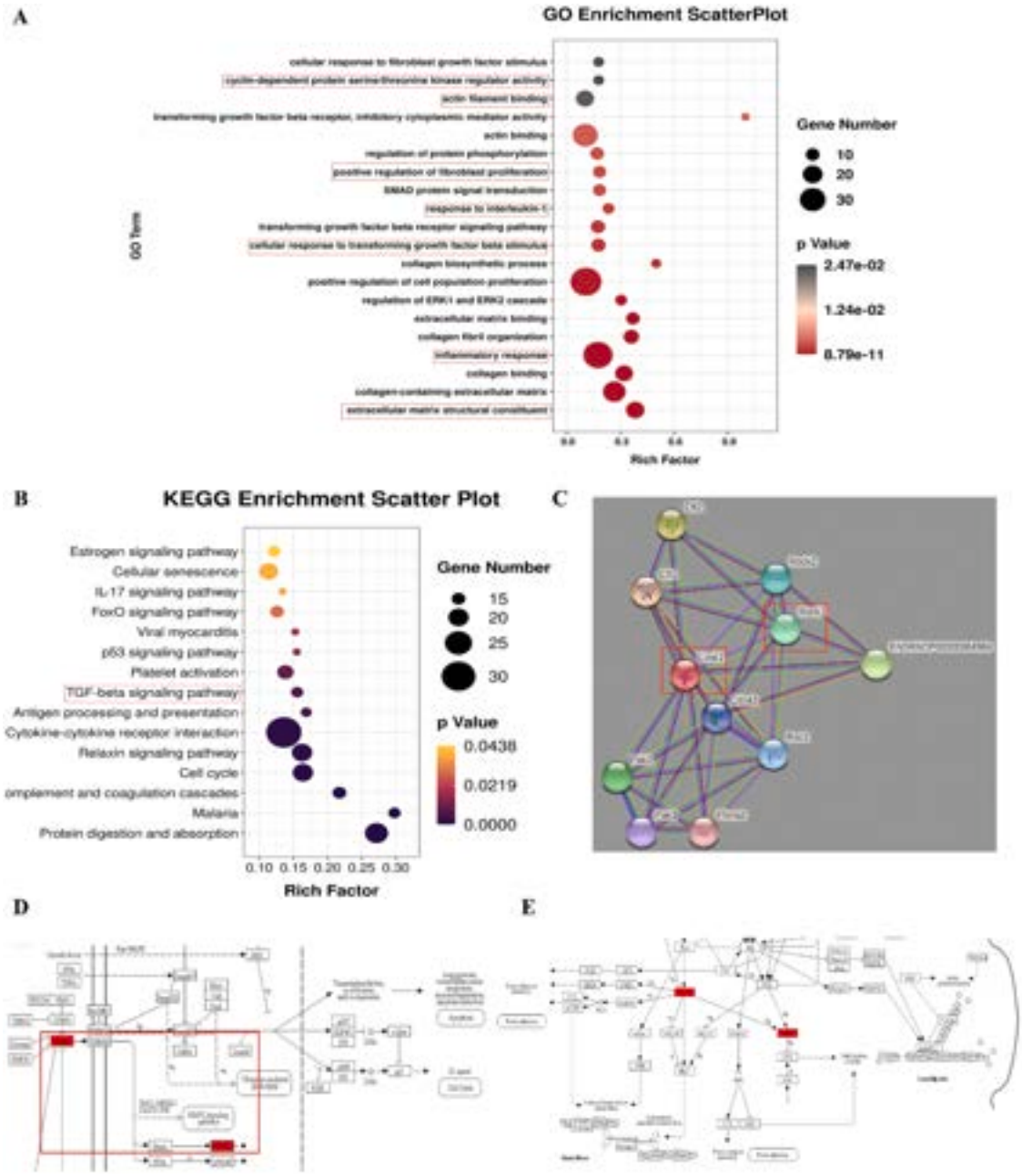


**Fig. 5.** RNA sequencing analysis of the signaling pathways associated with myocardial fibrosis and differential expression. A: GO enrichment map. Vertical coordinate: GO Term; horizontal coordinate: degree of enrichment (Rich factor); the bubble color indicates p-value; the bubble size indicates the number of differential genes belonging to a particular GO term; the larger the bubble, the greater the number of differential genes. B: KEGG enrichment map: vertical coordinate: KEGG pathway; horizontal coordinate: enrichment degree (Rich factor); the bubble color indicates p-value; the bubble size indicates the number of differential genes belonging to a certain KEGG pathway, and the larger the bubble, the higher the number of differential genes. C: Interaction diagram between ROCK1 and LIMK1. D, E: TGF-β1 signaling pathway.

extracted primary CFs, microscopic analysis revealed an inverted triangular or irregular morphology of the cells and the absence of their spontaneous pulsation, which confirmed that the extracts were CFs. The first-generation CFs were identified on the basis of the results of immunofluorescence staining with vimentin. The FSP-1 expression rate of $\geq$95% and almost zero α-SMA expression also confirmed that the CFs are first-generation CFs. Additionally, an analysis of the second-generation CFs indicated a decrease in vimentin and FSP-1 expression and an increase in the α-SMA protein level.

In the present study, the expression of CF and MFb markers, vimentin, and α-SMA proteins, was analyzed. Vimentin levels decreased with increased transmissibility, with a sharp decrease in vimentin expression noted in the second-generation CFs, whereas α-SMA protein expression increased. In summary, to ensure consistency in the experiments and their results, the first-generation cells were selected for subsequent experiments in this study (Supplementary Materials 2).

### 3.7. Determination of the dose and duration of NP and TGF-β1 exposure

TGF-β1 is currently recognized as a key mediator of the conversion of CFs into MFbs, which leads to fibrosis of CFs. In this study, after first-generation CFs were selected for stimulation with recombinant human TGF-β1, the CCK8 assay revealed that the CFs proliferated more significantly with an increase in the treatment duration and dose of the

recombinant factor. The proliferation rate of the CFs exposed to 10 ng/mL TGF-β1 for 24 h was higher than that of those exposed to 5 ng/mL TGF-β1 and blank. According to the immunofluorescence results, α-SMA expression was higher in the 10 ng/mL TGF-β1-treated cells. Therefore, 10 ng/mL TGF-β1 was selected as the modeling dose, and the treatment time was 24 h.

We investigated the effect of different NP concentrations at different treatment times, the CCK8 assay unveiled that the half-lethal dose ($IC_{50}$) of NP for CFs was 23.06 μmol/L. Therefore, 20 μmol/L was used as the NP concentration for subsequent transfection. Moreover, CF proliferation after NP exposure for 24 h was significantly higher than that after exposure for 6 and 12 h ($P < 0.05$), and therefore, the treatment time of 24 h was used for subsequent experiments. The cells were not affected by 0.01% DMSO (Li, 2019). Our results are similar to those of the previous study. Thus, we selected 0.01% DMSO to dissolve NP. The cells were grouped into blank, NP (20 μmol/L), and model (TGF-β1: 10 ng/mL) groups (Supplementary Materials 3).

### 3.8. Effects of NP exposure on myocardial fibrosis-related proteins and genes

We then investigated whether NP induces fibrosis in CFs. Cells in the blank group were shuttle-shaped and polygonal, whereas those in the NP and TGF-β1 groups were larger, wider, and irregularly shaped, with more pseudopods. Compared with the control group, the fluorescence expression of collagens I and III, MMP2, MMP9, and α-SMA increased in the NP and TGF-β1 groups (Fig. 6-A–F). Western blotting unveiled increased protein expression of fibrosis-related factors, including collagens I and III, MMP2, MMP9, α-SMA, IL-1β, and pro-IL-1β in the NP and TGF-β1 groups (Fig. 6-G–N). Gene expression analysis also revealed that collagen I and III, TGF-β1, and α-SMA mRNA levels were higher in the NP and TGF-β1 groups than in the blank group, confirming that NP-induced fibrosis in CFs (Fig. 6-O–R).

### 3.9. Effects of NP exposure on the TGF-β1/LIMK1 signaling pathway

According to the sequencing results, the TGF-β1/LIMK1 signaling pathway is involved in NP-induced myocardial fibrosis. To clarify the underlying mechanism, immunofluorescence staining and western blotting were performed. The results revealed that TGF-β1, LIMK1, P-LIMK1, Cofilin, and P-Cofilin expression was higher in the NP and TGF-β1 groups than in the blank group, which indicated that NP exposure activates the TGF-β1/LIMK1 signaling pathway (Fig. 7-A–K).

### 3.10. The working mechanism of the TGF-β1/LIMK1 signaling pathway in NP-induced CF fibrosis

The experimental results suggest that NP-induced CF fibrosis is related to TGF-β1/LIMK1 signaling pathway activation. To further investigate the regulatory role of this pathway in NP-induced CF fibrosis, we inhibited the TGF-β1/LIMK1 signaling pathway using a LIMK1-targeted inhibitor (BMS-5) and detected downstream protein expression. The expression of this signaling pathway and downstream proteins was subsequently detected by treating CFs with both BMS-5 and NP. Immunofluorescence and western blotting analyses revealed a lower LIMK1, P-LIMK1, Cofilin, and P-Cofilin expression in the BMS-5 group than in the blank group, indicating that BMS-5 effectively inhibited the TGF-β1/LIMK1 signaling pathway. Furthermore, TGF-β1, ROCK, RhoA, LIMK1, P-LIMK1, Cofilin, P-Cofilin, and α-SMA protein expression in the BMS-5+NP group was lower than that in the NP and TGF-β1 groups (Fig. 8-A–N). This indicated that the expression of NP-induced fibrosis-related proteins in CFs was suppressed following the inhibition of the TGF-β1/LIMK1 signaling pathway. The results demonstrate that NP can induce CF fibrosis by activating the aforementioned signaling pathway.

## 4. Discussion

By using a combination of biomarkers, including collagen protein expression, MMP disorder, abnormal expression of the transforming growth factor and inflammatory factor, etc., this study, for the first time, reported that perinatal NP exposure induced myocardial fibrosis in F1 male offspring. Moreover, we determined whether NP induces myocardial fibroblast fibrosis by using primary myocardial fibroblasts, as well as the role of the TGF-β1/LIMK1 signaling pathway in NP-induced myocardial fibrosis. In our previous study, subchronic NP exposure in rats resulted in myocardial fibrosis (Liu et al., 2021). However, whether growing and lactating infants directly exposed to NP, which is transmitted through the milk and placental barrier, develop myocardial fibrosis has not yet been reported. Body weight and the heart organ coefficient are key physiological indicators of bodily development. In this study, the heart organ coefficient of adult offspring rats was positively correlated with NP exposure during the perinatal period, which is not consistent with the previous study results (Yang et al., 2019). This may be attributable to species type, exposure dose, and gender differences. Epidemiological studies have demonstrated that, in NP-exposed animals, NP is found to be present in the blood (Russo et al., 2019), urine (Hou et al., 2021; Ringbeck et al., 2022), placenta (Huang et al., 2014), and breast milk (Shekhar et al., 2017; Sise and Uguz, 2017) of the mother rat during the perinatal period and blood of the offspring (Fu et al., 2022). This suggests that NP can be transferred to infants via the blood-brain barrier (BBB), placental barrier, and breast milk. This has been verified through HPLC experiments. In the present study, higher NP levels were found in the heart tissue and serum of the blank group, which may be related to the drinking water and feed provided to the rats, the solvent corn oil of NP, and the animal environment. This suggests that further studies are warranted to eliminate the effects of extraneous factors on the experiments so as to increase the accuracy of the results. Diastolic dysfunction is the most sensitive indicator of LV function in its early stage, while the ventricular wall thickness plays a unique role in CVD development and serves as a key indicator of cardiac dysfunction. Ejection fraction (EF) and fractional shortening (FS), important parameters reflecting cardiac systolic function, are widely recognized markers for evaluating cardiac function (Eisner et al., 2020; Huckstep et al., 2018). Our study revealed a significant decrease in EF and FS in offspring rats exposed to NP when compared to those in the blank control group, particularly within the ISO subgroup. Despite these findings, no statistically significant differences were observed among the various NP-exposed subgroups. This lack of significant variance may be attributed to the insensitivity of these traditional parameters to subtle changes in the function and structure of the offspring rats' hearts following NP exposure, leading to the absence of significant differences among the various NP subgroups. NP exposure increased LVAWs, LVAWd, LVPWs, and LVPWd, thereby suggesting that NP exposure induces cardiac dysfunction in adult offspring rats. Furthermore, NP transfer to infant rats through NP exposure during the perinatal period caused severe cardiac dysfunction in the offspring. A thorough discussion is required.

The study results revealed that NP exposure during the perinatal period altered collagen deposition in cardiac tissues and induced myocardial fibrosis through excessive collagen deposition, which is supported by the results of TEM characterization, and histopathological and immunohistochemical experiments. Mitochondria are a sensitive indicator of myocardial injury. In this study, the degree of disruption of mitochondrial vacuolization and fibrillar arrangement increased as the NP doses increased, which is consistent with the results of Perrotta et al (Perrotta and Tripepi, 2012). This indicates that pregnant and lactating mothers are extremely sensitive to toxic substances, and exposure to toxic substances even at low doses during this period induces toxic effects. These effects are often lifelong and irreversible and increase the myocardial fibrosis risk in the adult offspring. Classic Masson trichrome and Sirius Red staining for myocardial fibrosis revealed that NP

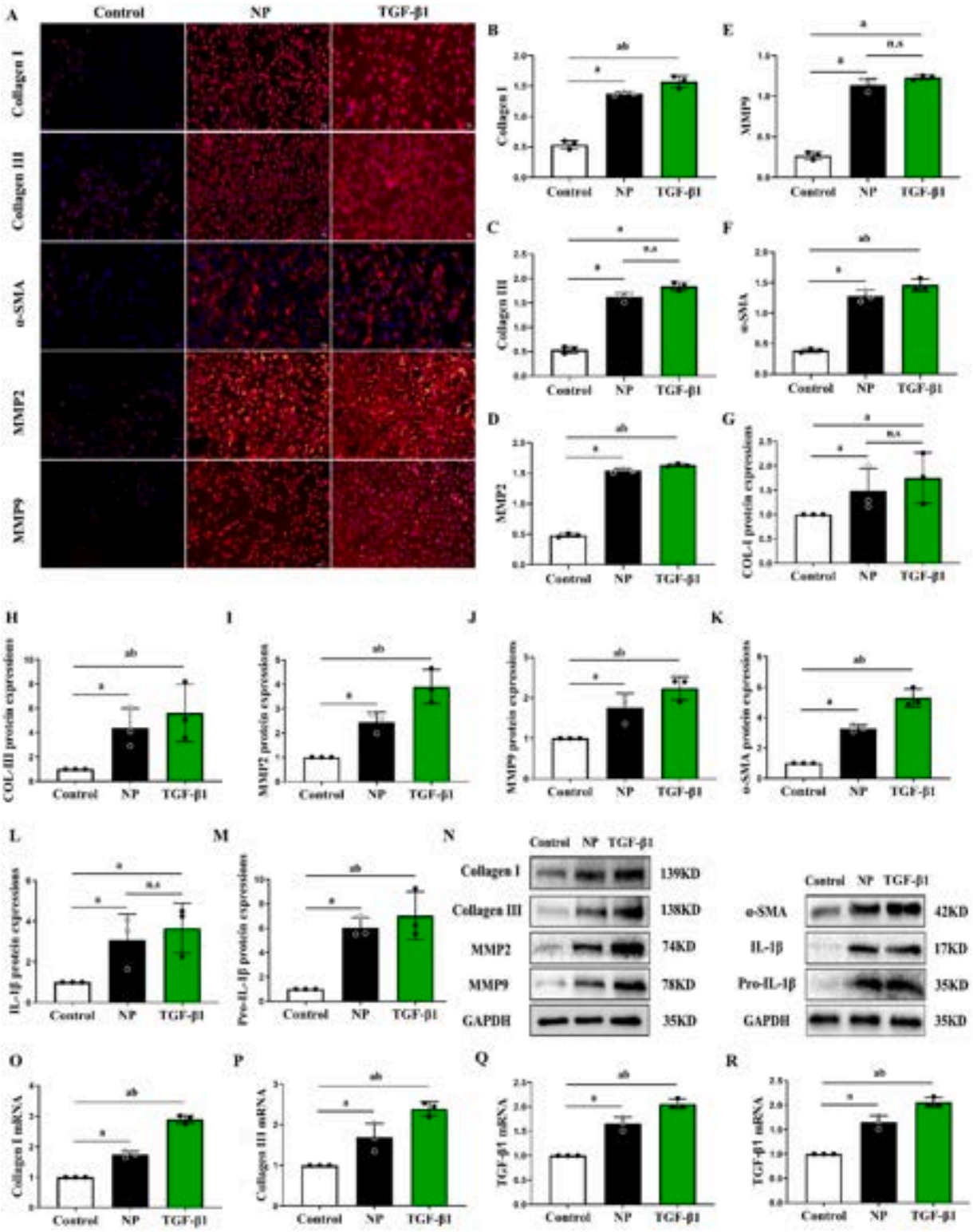


**Fig. 6.** Effects of NP exposure on proteins and genes related to myocardial fibrosis. A: Collagen I, Collagen III, α-SMA, MMP2 and MMP9 fluorescence, scale bar: 50 μm. B: Collagen I fluorescence expression, n = 3 (F = 151.259, $P < 0.001$). C: Collagen III fluorescence expression, n = 3 (F = 19.242, $P = 0.002$). D: α-SMA fluorescence expression, n = 3 (F = 48.894, $P < 0.001$). E: MMP2 fluorescence expression, n = 3 ($F_{MMP2} = 253.427$, $P < 0.001$). F: MMP9 fluorescence expression, n = 3 (F = 81.005, $P < 0.001$). G: Collagen I protein expression (F = 10.616, $P = 0.011$); H: Collagen III protein expression, n = 3 (F = 133.487, $P < 0.001$). I: MMP2 protein expression, n = 3 (F = 88.43, $P < 0.001$). J: MMP9 protein expression, n = 3 (F = 75.571, $P < 0.001$). K: α-SMA protein expression, n = 3 (F = 119.862, $P < 0.001$). L: IL-1β protein expression, n = 3 (F = 28.815, $P < 0.001$). M: Pro-IL-1β protein expression, n = 3 (F = 194.181 ; $P < 0.001$). N. Myocardial fibrosis-associated protein expressions in western blot analysis. O: Collagen I mRNA, n = 3 (F = 291.3, $P < 0.001$). P: Collagen III mRNA, n = 3 (F = 29.52, $P < 0.001$). Q: TGF-β1 mRNA, n = 3 (F = 94.09, $P < 0.001$). R: α-SMA mRNA, n = 3 (F = 170.5, $P < 0.001$). Data were expressed as $\overline{X} \pm SD$. Data were analyzed via one-way ANOVA and compared using LSD ([a]vs Control group, $P < 0.05$; [b]vs NP group, $P < 0.05$).

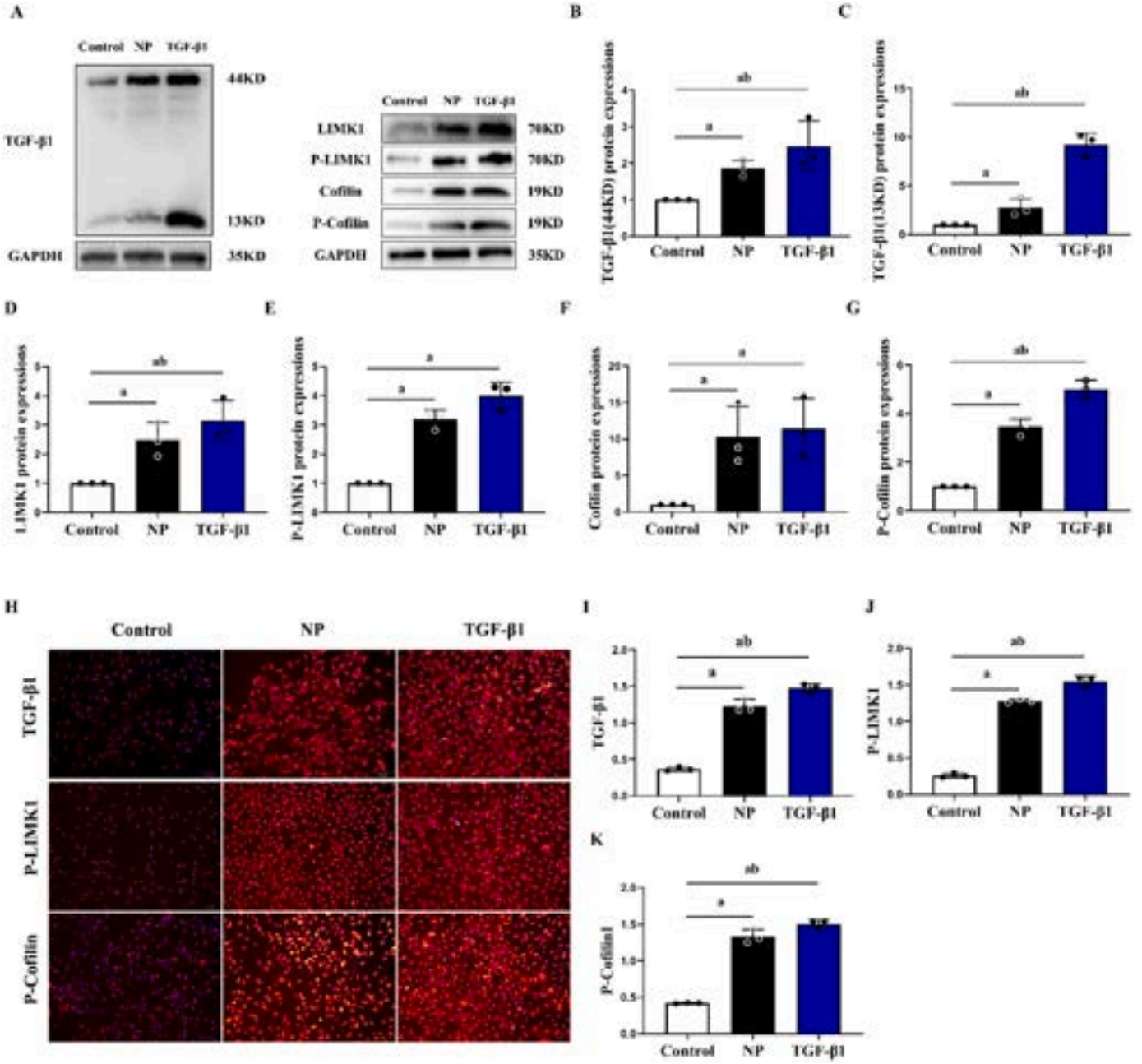


**Fig. 7.** Effects of NP exposure on the TGF-β1/LIMK1 signaling pathway. A: TGF-β1/LIMK1 signaling pathway associated protein expressions in western blot analysis. B: TGF-β1 44KD protein expression, n = 3 (F = 24.792 , $P < 0.001$). C: TGF-β1 13KD protein expression, n = 3 (F = 167.241, $P = 0.001$). D: LIMK1 protein expression, n = 3 (F = 41.066, $P < 0.001$). E: P-LIMK1 protein expression, n = 3 (F = 28.602 , $P = 0.001$). F: Cofilin protein expression, n = 3 (F = 45.371, $P < 0.001$); G: P-Cofilin protein expression, n = 3 (F = 32.826, $P = 0.001$). H: TGF-β1, P-LIMK1, *P*-Cofilin fluorescence, scale bar: 50 μm. I: TGF-β1 fluorescence, n = 3 (F = 88.346, $P < 0.001$). J: P-LIMK1 fluorescence, n = 3 (F = 260.368 , $P < 0.001$). K: P-Cofilin fluorescence, n = 3 (F = 80.065, $P < 0.001$). Data were expressed as $\overline{X} \pm$ SD. Data were analyzed using one-way ANOVA and compared via LSD ([a]vs Control group, $P < 0.05$; [b]vs NP group, $P < 0.05$).

exposure led to myocardial collagen deposition in adult littermates, which was consistent with the immunohistochemical analysis results. These results reaffirm that perinatal NP exposure causes cardiotoxicity in the litter, which agrees with the results of studies investigating myocardial fibrosis in adult rats with intrauterine exposure to di-(2-ethylhexyl) phthalate and nicotine-exposed pregnant rats (Dong et al., 2017; Zhao, 2014). These results demonstrated that NP exposure can cause pathological changes in the cardiac morphology and function of male adult offspring rats, which revealed the myocardial toxicity of NP, while the specific underlying mechanism remains unclear.

Perinatal NP exposure-induced myocardial fibrosis in adult rat offspring is supported by the expression of specific biomarkers. α-SMA is primarily expressed by MFb in pathological myocardial fibrosis, and a significant fibrosis-promoting cell phenotype is observed, thereby triggering an increased ECM level and abnormal expression of collagens I and III (Cao et al., 2020). This suggests that pro-fibrosis-promoting cytokines secreted by MFbs (e.g., collagens I and III, and α-SMA) play a key role in myocardial fibrosis. In the present study, both *in vitro* and *in vivo* experiments revealed that NP exposure can upregulate collagen I and III expression, which is consistent with the results of previous studies (Huang et al., 2014). However, the roles of other pro-fibrosis or fibrosis-promoting cytokines in NP-induced myocardial fibrosis are unknown. In a previous study, TGF-β1 enhanced MMP2 expression and further accelerated tumor cell invasion (Xie et al., 2017b). Another

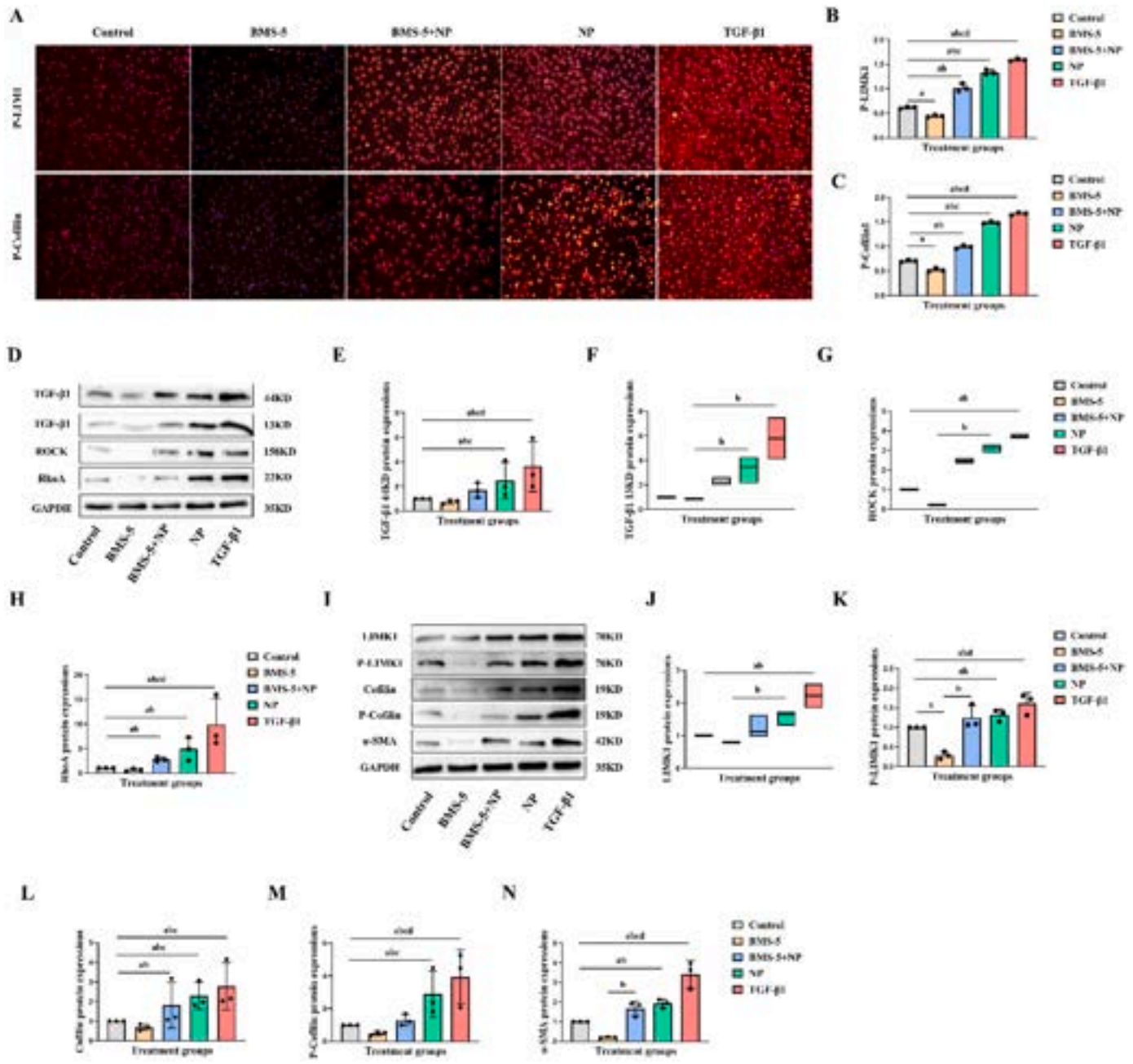


**Fig. 8.** The working mechanism of the TGF-β1/LIMK1 signaling pathway in NP-induced CFs fibrosis. A: P-LIMK1, P-Cofilin fluorescence, scale bar: 50 μm. B: P-LIMK1 fluorescence, n = 3 ($F = 317.205$ , $P < 0.001$). C: P-Cofilin fluorescence, n = 3 ($F = 604.647$, $P < 0.001$). D: TGF-β1/LIMK1 signaling pathway associated protein expressions in western blot analysis (TGF-β1, ROCK, RhoA). E: TGF-β1 44KD protein expression, n = 3 ($F = 24.389$, $P < 0.001$). F: TGF-β1 13KD protein expression, n = 3 ($H = 11.967$, $P = 0.018$).G: ROCK protein expression, n = 3 ($H = 21.314$, $P < 0.001$). H: RhoA protein expression, n = 3 ($F = 35.496$, $P < 0.001$). I: TGF-β1/LIMK1 signaling pathway associated protein expressions in western blot analysis (LIMK1, P-LIMK1, Cofilin, P-Cofilin, α-SMA). J: LIMK1 protein expression, n = 3 ($H = 12.433$, $P = 0.014$). K: P-LIMK1 protein expression, n = 3 ($F = 34.404$, $P < 0.001$). L: Cofilin protein expression, n = 3 ($F = 25.860$, $P < 0.001$). M: P-Cofilin protein expression, n = 3 ($F = 24.389$, $P < 0.001$). **N**: α-SMA protein expression, n = 3 ($F = 17.325$, $P < 0.001$). Data were expressed as $\overline{X} \pm$ SD B, C, E, H, K, L, M and N data were analyzed via one-way ANOVA and compared using LSD. F, G and J data were analyzed using Kruskal-Wallis test ([a]vs Control group, $P < 0.05$; [b]vs NP group, $P < 0.05$).

epidemiological study reported that serum MMP9 levels were significantly increased after myocardial fibrosis onset (Çelik et al., 2020). The present study demonstrated that MMP2 and MMP9 levels were also upregulated in the cardiac tissues and CFs of the NP-exposed rat pups, which further corroborates the findings of Kasneci et al (Kasneci et al., 2017b). Therefore, we suggest that NP-induced myocardial fibrosis is closely related to MMP levels. On analyzing the levels of IL-1β, a pro-fibrosis-related inflammatory indicator, the current study showed that both precursor and mature IL-1β levels significantly increased in the NP groups, strongly corroborating previous findings (Zhang et al., 2021b). This may be due to TGF-β1 activation in the body after NP stimulation, which triggers myocardial fibrosis by recruiting large quantities of inflammatory factors through TGF-β1. Thus, based on *in vivo* and *in vitro* experiments conducted in the present study, we concluded that NP exposure causes excessive collagen deposition, disruption of MMP homeostasis, massive release of inflammatory factors, and increased α-SMA expression, which results in myocardial fibrosis.

Regarding the underlying mechanism, KEGG and GO enrichment analyses revealed that NP-induced myocardial fibrosis is closely related to both the TGF-β1 signaling pathway as well as LIMK1. LIMK1 is a downstream effector of TGF-β1 that was differentially expressed. Nevertheless, the correlation of the aforementioned signaling pathway with NP-induced myocardial fibrosis will be further clarified. To date, few studies have investigated the induction of myocardial fibrosis by the TGF-β1/LIMK1 signaling pathway. In a recent study, the TGF-β1/LIMK1 signaling pathway was related to myocardial fibrosis occurrence, which indicated that TGF-β1, LIMK1, and Cofilin are highly expressed in myocardial fibrosis (Song, 2020). Therefore, we deduced that the TGF-β1/LIMK1 signaling pathway plays a vital role in myocardial fibrosis. In this study, NP exposure significantly increased the TGF-β1 level. Because TGF-β1 activation activates the LIMK1 signaling pathway in cells, the TGF-β1/LIMK1 signaling pathway was concluded to be involved in NP-induced myocardial fibrosis. To further test our hypothesis, a LIMK1 inhibitor (BMS-5) was used here to inhibit this signaling pathway. BMS-5 effectively inhibited the TGF-β1/LIMK1 signaling pathway and partially inhibited the upregulation of NP-induced fibrosis-related protein expression in CFs. According to a recent study, LIMK1 was upregulated in atrial fibrosis, whereas downregulated LIMK1 effectively inhibited the conversion of recombinant human TGF-β1-induced CFs to MFbs. This reduced excessive ECM deposition, which strongly corroborates the present study results (Chen et al., 2019). Notably, although LIMK1 was the target of BMS-5, the upstream proteins TGF-β1, ROCK, and RhoA in the TGF-β/LIMK1 signaling pathway were also inhibited. We speculate that this is caused by negative feedback following the inhibition of the TGF-β1/LIMK1 signaling pathway, or the role of BMS-5 in inhibiting the synthesis of TGF-β1, ROCK, and RhoA components. In summary, *in vitro* experiments validated our hypothesis that NP induces fibrosis in CFs by activating and upregulating the TGF-β1/LIMK1 signaling pathway and related proteins downstream. In summary, the novel effect of NP exposure on the regulation of CF differentiation to MFbs was determined. Indeed, this effect was realized through NP-induced activation of the TGF-β1/LIMK1 signaling pathway, which leads to myocardial fibrosis. This study offers a novel mechanism of NP-induced myocardial fibrosis and is of great significance for developing intervention measures for NP exposure-induced CVDs.

## 5. Conclusion

In this study, histopathological changes were observed in the hearts of male adult rats exposed to NP during the perinatal period. Alterations were detected in myocardial fibrosis-related protein and gene expression. Perinatal NP exposure induced myocardial fibrosis in male adult rats. Cellular assays revealed that NP directly or indirectly contributed to excessive CF proliferation, thereby leading to fibrosis. Inhibition of the TGF-β1/LIMK1 signaling pathway also abrogated NP-induced fibrosis in the CFs. NP upregulated the expression of this signaling pathway and related proteins downstream by activating the aforementioned pathway. Thus, the TGF-β1/LIMK1 signaling pathway may be a critical regulatory pathway in NP-induced myocardial fibrosis.

## Ethics statement

This experiment was approved the Animal Experiment Ethics Committee of Zunyi Medical University [No. Lun Shen (2020) 2–359]. All experiments were conducted under the guidelines and regulations of Zunyi Medical University.

## CRediT authorship contribution statement

**Liu Weichu:** Investigation. **Aris Ahmad Zaharin:** Data curation. **Long Xianping:** Methodology, Resources. **Guo Mei:** Data curation, Formal analysis, Investigation, Methodology, Software, Validation, Visualization, Writing – original draft. **Xu Jie:** Conceptualization, Data curation, Funding acquisition, Methodology, Project administration, Validation, Writing – review & editing, Supervision. **Xu Yuzhu:** Data curation. **Yu Jie:** Conceptualization, Data curation, Formal analysis, Funding acquisition, Methodology, Project administration, Resources, Supervision, Validation, Visualization, Writing – original draft, Writing – review & editing, Investigation. **Yang Danli:** Methodology. **Luo Ya:** Methodology.

## Declaration of Competing Interest

The authors declare that they have no known competing financial interests or personal relationships that could have appeared to influence the work reported in this paper.

## Data Availability

Data will be made available on request.

## Acknowledgements

This work was supported by the National Natural Science Foundation of China (22266039, 22166035); Guizhou High-Level Innovative Talent Support Program ([2020]6014, GCC[2022]035-1). Fund of Department of Science and Technology of Guizhou Province, China (ZK[2023]493). Science and Technology Foundation of the Health Commission of Guizhou Province (gzwkj2024-218). Key Program of Scientific and Technological Fund of Department of Science and Technology of Guizhou Province, China (2024).

## Appendix A. Supporting information

Supplementary data associated with this article can be found in the online version at doi:10.1016/j.ecoenv.2024.116110.

## References

Broughton, K.M., Wang, B.J., Firouzi, F., Khalafalla, F., Dimmeler, S., Fernandez-Aviles, F., Sussman, M.A., 2018. Mechanisms of Cardiac Repair and Regeneration. Circ. Res. 122, 1151–1163. https://doi.org/10.1161/CIRCRESAHA.117.312586.

Cao, J.W., Duan, S.Y., Zhang, H.X., Chen, Y., Guo, M., 2020. Zinc deficiency promoted fibrosis via ROS and TIMP/MMPs in the Myocardium of Mice. Biol. Trace Elem. Res 196, 145–152. https://doi.org/10.1007/s12011-019-01902-4.

Çelik, Ö., Şahin, A.A., Sarıkaya, S., Uygur, B., 2020. Correlation between serum matrix metalloproteinase and myocardial fibrosis in heart failure patients with reduced ejection fraction: A retrospective analysis. Anatol. J. Cardiol. 24, 303–308. https://doi.org/10.14744/AnatolJCardiol.2020.54937.

Chen, Q., Gimple, R.C., Li, G., Chen, J., Wu, H., Li, R., Xie, J., Xu, B., 2019. LIM kinase 1 acts as a profibrotic mediator in permanent atrial fibrillation patients with valvular heart disease. J. Biosci. 44 (1), 16.

Chen, J.Y., Liu, Z.P., Huo, J., Yue, Q.L., Bao, H.H., Zhang, L.S., 2018. Discussion of tolerable daily intake for nonylphenol. Chin. J. Food Hyg. 30, 104–108. https://doi.org/10.13590/j.cjfh.2018.01.022.

Chowdhury, Dhrubajyoti, Hell, Johannes W., 2019. Ca2+/calmodulin binding to PSD-95 downregulates its palmitoylation and AMPARs in long-term depression. Front Synaptic Neurosci. 11, 6. https://doi.org/10.3389/fnsyn.2019.00006.

Cunny, H.C., Mayes, B.A., Rosica, K.A., Trutter, J.A., Van Miller, J.P., 1997. Subchronic toxicity (90-day) study with para-nonylphenol in rats. Regul. Toxicol. Pharm. 26, 172–178. https://doi.org/10.1006/rtph.1997.1154.

Díez, J., González, A., Kovacic, J.C., 2020. Myocardial interstitial fibrosis in nonischemic heart disease, Part 3/4: JACC focus seminar. J. Am. Coll. Cardiol. 75, 2204–2218. https://doi.org/10.1016/j.jacc.2020.03.019.

Dong, W.J., Li, X.N., Xia, Z.H., Zhang, Y.J., 2017. Prenatal nicotine exposure induces cardiac fibrosis in adult male offspnng. Chin. J. Pharm. Toxicol. 31, 621–625. https://doi.org/10.3867/j.issn.1000-3002.2017.06.018.

Eisner, D.A., Caldwell, J.L., Trafford, A.W., Hutchings, D.C., 2020. The control of diastolic calcium in the heart: basic mechanisms and functional implications. Circ. Res. 126, 395–412. https://doi.org/10.1161/CIRCRESAHA.119.315891.

Fu, X., He, J., Zheng, D., Yang, X., Wang, P., Tuo, F., Wang, L., Li, S., Xu, J., Yu, J., 2022. Association of endocrine disrupting chemicals levels in serum, environmental risk factors, and hepatic function among 5- to 14-year-old children. Toxicology 465, 153011. https://doi.org/10.1016/j.tox.2021.153011.

Fu, X., Xu, J., Zhang, R., Yu, J., 2020. The association between environmental endocrine disruptors and cardiovascular diseases: a systematic review and meta-analysis. Environ. Res 187, 109464. https://doi.org/10.1016/j.envres.

Gao, Q., Liu, S., Guo, F., Liu, S., Yu, X., Hu, H., Sun, X., Hao, L., Zhu, T., 2015. Nonylphenol affects myocardial contractility and L-type Ca(2+) channel currents in a non-monotonic manner via G protein-coupled receptor 30. Toxicology 334, 122–129. https://doi.org/10.1016/j.tox.2015.06.004.

García-Arévalo, M., Lorza-Gil, E., Cardoso, L., Batista, T.M., Araujo, T.R., Ramos, L.A.F., Areas, M.A., Nadal, A., Carneiro, E.M., Davel, A.P., 2021a. Ventricular fibrosis and coronary remodeling following short-term exposure of healthy and malnourished mice to bisphenol A. Front Physiol. 12, 638506 https://doi.org/10.3389/fphys.2021.638506.

García-Arévalo, M., Lorza-Gil, E., Cardoso, L., Batista, T.M., Araujo, T.R., Ramos, L.A.F., Areas, M.A., Nadal, A., Carneiro, E.M., Davel, A.P., 2021b. Ventricular fibrosis and coronary remodeling following short-term exposure of healthy and malnourished mice to bisphenol A. Front Physiol. 12, 638506 https://doi.org/10.3389/fphys.2021.638506.

Hou, Y., Li, S., Xia, L., Yang, Q., Zhang, L., Zhang, X., Liu, H., Huo, R., Cao, G., Huang, C., Tian, X., Sun, L., Cao, D., Zhang, M., Zhang, Q., Tang, N., 2021. Associations of urinary phenolic environmental estrogens exposure with blood glucose levels and gestational diabetes mellitus in Chinese pregnant women. Sci. Total Environ. 754, 142085 https://doi.org/10.1016/j.scitotenv.2020.142085.

Huang, Y.F., Wang, P.W., Huang, L.W., Yang, W., Yu, C.J., Yang, S.H., Chiu, H.H., Chen, M.L., 2014. Nonylphenol in pregnant women and their matching fetuses: placental transfer and potential risks of infants. Environ. Res. 134, 143–148. https://doi.org/10.1016/j.envres.2014.07.004.

Huang, J.B., Wu, Y.P., Lin, Y.Z., Cai, H., Chen, S.H., Sun, X.L., Li, X.D., Wei, Y., Zheng, Q. S., Xu, N., Xue, X.Y., 2020. Up-regulation of LIMK1 expression in prostate cancer is correlated with poor pathological features, lymph node metastases and biochemical recurrence. J. Cell Mol. Med 24, 4698–4706. https://doi.org/10.1111/jcmm.15138.

Huckstep, O.J., Williamson, W., Telles, F., Burchert, H., Bertagnolli, M., Herdman, C., Arnold, L., Smillie, R., Mohamed, A., Boardman, H., McCormick, K., Neubauer, S., Leeson, P., Lewandowski, A.J., 2018. Physiological stress elicits impaired left ventricular function in preterm-born adults. J. Am. Coll. Cardiol. 71, 1347–1356. https://doi.org/10.1016/j.jacc.2018.01.046.

Jiang, J., Liang, S., Zhang, J., Du, Z., Xu, Q., Duan, J., Sun, Z., 2021. Melatonin ameliorates PM -induced cardiac perivascular fibrosis through regulating mitochondrial redox homeostasis. J. Pineal Res 70, e12686. https://doi.org/10.1111/jpi.12686.

Kang, X., Li, W., Liu, W., Liang, H., Deng, J., Wong, C.C., Zhao, S., Kang, W., To, K.F., Chiu, P.W.Y., Wang, G., Yu, J., Ng, E.K.W., 2021. LIMK1 promotes peritoneal metastasis of gastric cancer and is a therapeutic target. Oncogene 40, 3422–3433. https://doi.org/10.1038/s41388-021-01656-1.

Kasneci, A., Lee, J.S., Yun, T.J., Shang, J., Lampen, S., Gomolin, T., Cheong, C.C., Chalifour, L.E., 2017a. From the cover: lifelong exposure of C57bl/6n male mice to bisphenol a or bisphenol s reduces recovery from a myocardial infarction. Toxicol. Sci. 159, 189–202. https://doi.org/10.1093/toxsci/kfx133.

Kasneci, A., Lee, J.S., Yun, T.J., Shang, J., Lampen, S., Gomolin, T., Cheong, C.C., Chalifour, L.E., 2017b. From the cover: lifelong exposure of C57bl/6n male mice to bisphenol a or bisphenol s reduces recovery from a myocardial infarction. Toxicol. Sci. 159, 189–202. https://doi.org/10.1093/toxsci/kfx133.

Liu, C., Ni, C., Liu, W., Liu, W.C., Yang, X.L., Yu, J., 2021. Effects of long-term nonylphenol exposure on myocardial fibrosis and cardiac function in rats. Environ. Sci. Eur. 33. https://doi.org/10.21203/rs.3.rs-142059/v1.

Li, Y., Song, D., Mao, L., Abraham, D.M., Bursac, N., 2020. Lack of Thy1 defines a pathogenic fraction of cardiac fibroblasts in heart failure. Biomaterials 236, 119824. https://doi.org/10.1016/j.biomaterials.2020.119824.

Li, C., Zhang, J., Xue, M., Li, X., Han, F., Liu, X., Xu, L., Lu, Y., Cheng, Y., Li, T., Yu, X., Sun, B., Chen, L., 2019. SGLT2 inhibition with empagliflozin attenuates myocardial oxidative stress and fibrosis in diabetic mice heart. Cardiovasc Diabetol. 18, 15. https://doi.org/10.1186/s12933-019-0816-2.

Li W.M. (2019) Nonylphenol induced rat obesity and promotion of differentiation of 3T3-L1 preadipocytes. Master thesis. Zunyi Medical University, Guizhou.

Lu J.W. (2019) Toxicological Effects of Hexavalent Chromium on the Heart of Chinese Rural Dog. Master thesis. Shandong Agricultural University, Shandong.

Lu, Z., Gan, J., 2014. Analysis, toxicity, occurrence and biodegradation of nonylphenol isomers: a review. Environ. Int. 73, 334–345. https://doi.org/10.1016/j.envint.2014.08.017.

Medzikovic, L., Heese, H., van Loenen, P.B., van Roomen, C.P.A.A., Hooijkaas, I.B., Christoffels, V.M., Creemers, E.E., de Vries, C.J.M., de Waard, V., 2021. Nuclear receptor Nur77 controls cardiac fibrosis through distinct actions on fibroblasts and cardiomyocytes. Int J. Mol. Sci. 22, 1600. https://doi.org/10.3390/ijms22041600.

Nagao, T., Wada, K., Marumo, H., Yoshimura, S., Ono, H., 2001. Reproductive effects of nonylphenol in rats after gavage administration: a two-generation study. Reprod. Toxicol. 15, 293–315. https://doi.org/10.1016/s0890-6238(01)00123-x.

Park, S., Ranjbarvaziri, S., Lay, F.D., Zhao, P., Miller, M.J., Dhaliwal, J.S., Huertas-Vazquez, A., Wu, X., Qiao, R., Soffer, J.M., Rau, C., Wang, Y., Mikkola, H.K.A., Lusis, A.J., Ardehali, R., 2018. Genetic regulation of fibroblast activation and proliferation in cardiac fibrosis. Circulation 138, 1224–1235. https://doi.org/10.1161/CIRCULATIONAHA.118.035420.

Patel, B.B., Kasneci, A., Bolt, A.M., Di Lalla, V., Di Iorio, M.R., Raad, M., Mann, K.K., Chalifour, L.E., 2015. Chronic exposure to bisphenol a reduces successful cardiac remodeling after an experimental myocardial infarction in male C57bl/6n mice. Toxicol. Sci. 146, 101–115. https://doi.org/10.1093/toxsci/kfv073.

Perrotta, I., Tripepi, S., 2012. Ultrastructural alterations in the ventricular myocardium of the adult Italian newt (Lissotriton italicus) following exposure to nonylphenol ethoxylate. Micron 43, 183–191. https://doi.org/10.1016/j.micron.2011.07.011.

Radhiga, T., Senthil, S., Sundaresan, A., Pugalendi, K.V., 2019. Ursolic acid modulates MMPs, collagen-I, α-SMA, and TGF-β expression in isoproterenol-induced myocardial infarction in rats. Hum. Exp. Toxicol. 38, 785–793. https://doi.org/10.1177/0960327119842620.

Ringbeck, B., Bury, D., Ikeda-Araki, A., Ait Bamai, Y., Ketema, R.M., Miyashita, C., Brüning, T., Kishi, R., Koch, H.M., 2022. Nonylphenol exposure in 7-year-old Japanese children between 2012 and 2017- estimation of daily intakes based on novel urinary metabolites. Environ. Int. 161, 107145 https://doi.org/10.1016/j.envint.2022.107145.

Russo, G., Barbato, F., Mita, D.G., Grumetto, L., 2019. Simultaneous determination of fifteen multiclass organic pollutants in human saliva and serum by liquid chromatography-tandem ultraviolet/fluorescence detection: a validated method. Biomed. Chromatogr. 33, e4427 https://doi.org/10.1002/bmc.4427.

Shan, J., Jiang, B., Yu, B., Li, C., Sun, Y., Guo, H., Wu, J., Klumpp, E., Schäffer, A., Ji, R., 2011. Isomer-specific degradation of branched and linear 4-nonylphenol isomers in an oxic soil. Environ. Sci. Technol. 45, 8283–8289. https://doi.org/10.1021/es200224c.

Shekhar, S., Sood, S., Showkat, S., Lite, C., Chandrasekhar, A., Vairamani, M., Barathi, S., Santosh, W., 2017. Detection of phenolic endocrine disrupting chemicals (EDCs) from maternal blood plasma and amniotic fluid in Indian population. Gen. Comp. Endocrinol. 241, 100–107. https://doi.org/10.1016/j.ygcen.2016.05.025.

Sise, S., Uguz, C., 2017. Nonylphenol in human breast milk in relation to sociodemographic variables, diet, obstetrics histories and lifestyle habits in a turkish population. Iran. J. Public Health 46, 491–499.

Song J. (2020) Study on the effect of Jiedu Tongluo Fang on Myocardial fibrosis in rats based on TGF-β1/LIMK1 signaling pathway. Ph.D thesis. Changchun University of Traditional Chinese Medicine, Jilin.

Travers, J.G., Kamal, F.A., Robbins, J., Yutzey, K.E., Blaxall, B.C., 2016. Cardiac fibrosis: the fibroblast awakens. Circ. Res. 118, 1021–1040. https://doi.org/10.1161/CIRCRESAHA.115.306565.

Wang, L., Guo, M., Feng, G., Wang, P., Xu, J., Yu, J., 2021. Effects of chronic exposure to nonylphenol at environmental concentration on thyroid function and thyroid hyperplasia disease in male rats. Toxicology 461, 152918. https://doi.org/10.1016/j.tox.2021.152918.

Wang, G., Wang, R., Ruan, Z., Liu, L., Li, Y., Zhu, L., 2020a. MicroRNA-132 attenuated cardiac fibrosis in myocardial infarction-induced heart failure rats. Biosci. Rep. 40, BSR20201696 https://doi.org/10.1042/BSR20201696.

Wang, L., Xu, J., Zeng, F., Fu, X., Xu, W., Yu, J., 2019. Influence of nonylphenol exposure on basic growth, development, and thyroid tissue structure in F1 male rats. PeerJ 7, e7039. https://doi.org/10.7717/peerj.7039.

Wan, E.Y.F., Fung, W.T., Schooling, C.M., Au Yeung, S.L., Kwok, M.K., Yu, E.Y.T., Wang, Y., Chan, E.W.Y., Wong, I.C.K., Lam, C.L.K., 2021. Blood pressure and risk of cardiovascular disease in UK biobank: a mendelian randomization study. Hypertension 77, 367–375. https://doi.org/10.1161/HYPERTENSIONAHA.120.16138.

Xiao, Y., Zhao, J., Tuazon, J.P., Borlongan, C.V., Yu, G., 2019. MicroRNA-133a and myocardial infarction. Cell Transpl. 28, 831–838. https://doi.org/10.1177/0963689719843806.

Xie, J., Li, X., Zhang, W., Chai, X., Huang, Y., Li, K., Cheng, X., Zhao, S., 2017a. Aberrant expression of LIMK1 impairs neuronal migration during neocortex development. Histochem Cell Biol. 147, 471–479. https://doi.org/10.1007/s00418-016-1514-8.

Xie, J., Tu, T., Zhou, S., Liu, Q., 2017b. Transforming growth factor (TGF)-β1 signal pathway: a promising therapeutic target for attenuating cardiac fibrosis. Int. J. Cardiol. 239, 9. https://doi.org/10.1016/j.ijcard.2017.02.032.

Yang, Y.J., Liu, C., Chen, N.H., Xu, J., 2019. Effects of nonylphenol exposure on myocardial tissue of SD rats, 2593-2595+2599 J. Mod. Med. Health 35. https://doi.org/10.3969/j.issn.1009-5519.2019.17.001.

Yu, J., Li, W., Tang, L., Luo, Y., Xu, J., 2020a. In vivo and in vitro effects of chronical exposure to nonylphenol on lipid metabolism. Environ. Sci. Eur. https://doi.org/10.1186/s12302-020-00364-z.

Yu, J., Tuo, F., Luo, Y., Yang, Y., Xu, J., 2020b. Toxic effects of perinatal maternal exposure to nonylphenol on lung inflammation in male offspring rats. Sci. Total Environ. 737, 139238 https://doi.org/10.1016/j.scitotenv.2020.139238.

Yu, J., Tuo, F., Luo, Y., Yang, Y., Xu, J., 2020c. Toxic effects of perinatal maternal exposure to nonylphenol on lung inflammation in male offspring rats. Sci. Total Environ. 737, 139238 https://doi.org/10.1016/j.scitotenv.2020.139238.

Yu, J., Wang, P., Yan, W.X., Gao, F., He, L.T., Li, W.M., Xu, J., 2017. The effects of gestational and lactational exposure to Nonylphenol on c-jun, and c-fos expression and learning and memory in hippocampus of male F1 rat. Iran. J. Basic Med. Sci. 20, 386–391. https://doi.org/10.22038/IJBMS.2017.8578.

Yu, J., Yang, X.F., Yang, M.X., Yang, X.S., Yang, J., Tang, Y., Xu, J., 2016. Mechanism of nonylphenol-induced neurotoxicity in F1 rats during sexual maturity. Wien. Klin. Woche 128, 426–434. https://doi.org/10.1007/s00508-016-0960-6.

Zhang, W.J., Chen, S.J., Zhou, S.C., Wu, S.Z., Wang, H., 2021b. Inflammasomes and fibrosis. Front Immunol. 12, 643149 https://doi.org/10.3389/fimmu.2021.643149.

Zhao Q.S. (2014) Maternal in utero exposure to di-(2-ethylhexyl) phthalate affects the heart of adult female offspring. Anhui Medical University, Anhui.

Zhao, X.H., Laschinger, C., Arora, P., Szászi, K., Kapus, A., McCulloch, C.A., 2007. Force activates smooth muscle alpha-actin promoter activity through the Rho signaling pathway. J. Cell Sci. 120, 1801–1809. https://doi.org/10.1242/jcs.001586.

Zhou, W., Young, J.L., Men, H., Zhang, H., Yu, H., Lin, Q., Xu, H., Xu, J., Tan, Y., Zheng, Y., Cai, L., 2022. Sex differences in the effects of whole-life, low-dose cadmium exposure on postweaning high-fat diet-induced cardiac pathogeneses. Sci. Total Environ. 809, 152176 https://doi.org/10.1016/j.scitotenv.2021.152176.